NASA CR-134871

ANNUAL REPORT

THEORETICAL INVESTIGATIONS OF PLASMA PROCESSES IN THE ION BOMBARDMENT THRUSTER

Prepared for
LEWIS RESEARCH CENTER
NATIONAL AERONAUTICS AND SPACE ADMINISTRATION
Grant NGR-06-002-147

October 1975

Department of Electrical Engineering
Colorado State University
Fort Collins, Colorado

1. Report No. NASA CR-134871	2. Government Accession No.	3. Recipient's Catalog No.

4. Title and Subtitle

Theoretical Investigation of Plasma Processes in the
Ion Bombardment Thruster

5. Report Date
October 1975

6. Performing Organization Code

7. Author(s)

H. E. Wilhelm

8. Performing Organization Report No.

10. Work Unit No.

9. Performing Organization Name and Address

Department of Electrical Engineering
Colorado State University
Fort Collins, Colorado 80523

11. Contract or Grant No.
NGR 06-002-147

13. Type of Report and Period Covered
Contractor Report
1 July 74 - 1 September 75

12. Sponsoring Agency Name and Address

National Aeronautics and Space Administration
Washington, D.C. 20546

14. Sponsoring Agency Code

15. Supplementary Notes

Grant Manager, Maris Mantenieks
Spacecraft Technology Division
NASA Lewis Research Center
Cleveland, OH 44135

16. Abstract

A physical model for a thruster discharge is developed consisting of a spatially diverging plasma sustained electrically between a small ring cathode and a larger ring anode in a cylindrical chamber with an axial magnetic field. The associated boundary-value problem for the coupled partial differential equations with mixed boundary conditions, which describe the electric potential and the plasma velocity fields, is solved in closed form. The spatial structure of the discharge fields is illustrated in 45 figures.

By means of quantum-mechanical perturbation theory, a formula for the number S(E) of atoms sputtered on the average by an ion of energy E is derived from first principles. As an application mercury-metal atom scattering cross sections are determined by quantitative comparison of the theoretical and experimental S(E)-values for sputtering mercury ions and various metals, such as Ag, Au, Co, Cu, Fe, Mo, Nb, Pt, Ta, Ti, W, Zr.

The boundary-value problem describing the diffusion of the sputtered atoms through the surrounding rarefied electron-ion plasma to the system surfaces of ion propulsion systems is formulated and treated analytically. It is shown that outer boundary-value problems of this type lead to a complex integral equation, which requires numerical resolution.

17. Key Words (Suggested by Author(s))	18. Distribution Statement
Ion Bombardment Thruster Thruster Discharge Theory Sputtering Theory Deposition Analysis	Unclassified - Unlimited

19. Security Classif. (of this report)	20. Security Classif. (of this page)	21. No. of Pages	22. Price*
Unclassified	Unclassified	104	$3.00

* For sale by the National Technical Information Service, Springfield, Virginia 22151

CONTENTS

INTRODUCTION

The Grant NGR-06-002-147, "Theoretical Investigations of Plasma Processes in the Ion Bombardment Thruster," is concerned with i) the sputtering of the accelerating grid, and the cathodes of the hollow cathode and neutralizer discharges, ii) the deposition of the sputtered atoms on system components such as the solar energy collectors, and iii) the analysis of the thruster discharge. The progress made on these subject in the period from 7.1.74 to 8.30.75 is communicated herein.

A physical model for a thruster discharge is developed consisting of spatially diverging plasma sustained electrically between a small ring cathode and a larger ring anode in a cylindrical chamber with an axial magnetic field. The associated boundary-value problem for the coupled partial differential equations with mixed boundary conditions is solved in closed form for the electric potential, the electric field, current density, and velocity distribution. As a result of the Lorentz forces, the plasma rotates with speeds of the order 10^6 cm/sec around the chamber axis. It is shown that at sufficiently large Hall coefficients and/or Hartmann numbers i) the radial spreading of the discharge is reduced by the external magnetic field, and ii) the discharge fields exhibit an oscillatory spatial structure off the discharge axis, e.g., current flows in alternating axial directions.

By means of quantum-mechanical perturbation theory, a formula for the number S(E) of atoms sputtered on the average by an ion of energy E is derived from first principles. The theory agrees with experimental sputtering data in the low energy region above the threshold, and leads to the correct sputtering thresholds. As an application mercury-metal atom scattering cross sections are determined by quantitative comparison of the theortetical and experimental S(E)-values for sputtering mercury ions and polycrystalline target materials, such as Ag, Au, Co, Cu, Fe, Mo,Nb,Pt, Ta, Ti, W, and Zr.

The boundary-value problem describing the diffusion of the sputtered atoms through the surrounding rarefied electron-ion plasma of ion propulsion systems to the system surfaces is formulated and treated analytically. It is shown that outer boundary-value problems of this type lead to a complicated integral equation. Numerical results can be obtained by a considerable computer effort.

The investigations reported herein represent preliminary communications. The final version of this work will be communicated in form of publications at a later date.

THEORY OF ROTATING DISCHARGE IN MAGNETIC FIELD

ABSTRACT

A physical model for a thruster discharge is developed consisting of a spatially diverging plasma sustained electrically between a small ring cathode and a larger ring anode in a cylindrical chamber with an axial magnetic field. The associated boundary-value problem for the coupled partial differential equations with mixed boundary conditions, which describe the electric potential and the plasma velocity fields, is solved in closed form. The electric field, current density, and velocity distributions are discussed in terms of the Hartmann number H and the Hall coefficient $\omega\tau$. It is shown that the plasma fields exhibit an oscillatory radial structure at sufficiently large magnetic interaction parameters H and $\omega\tau$. As a result of the Lorentz forces, the plasma rotates with speeds as high as 10^6 cm/sec around its axis of symmetry at typical conditions.

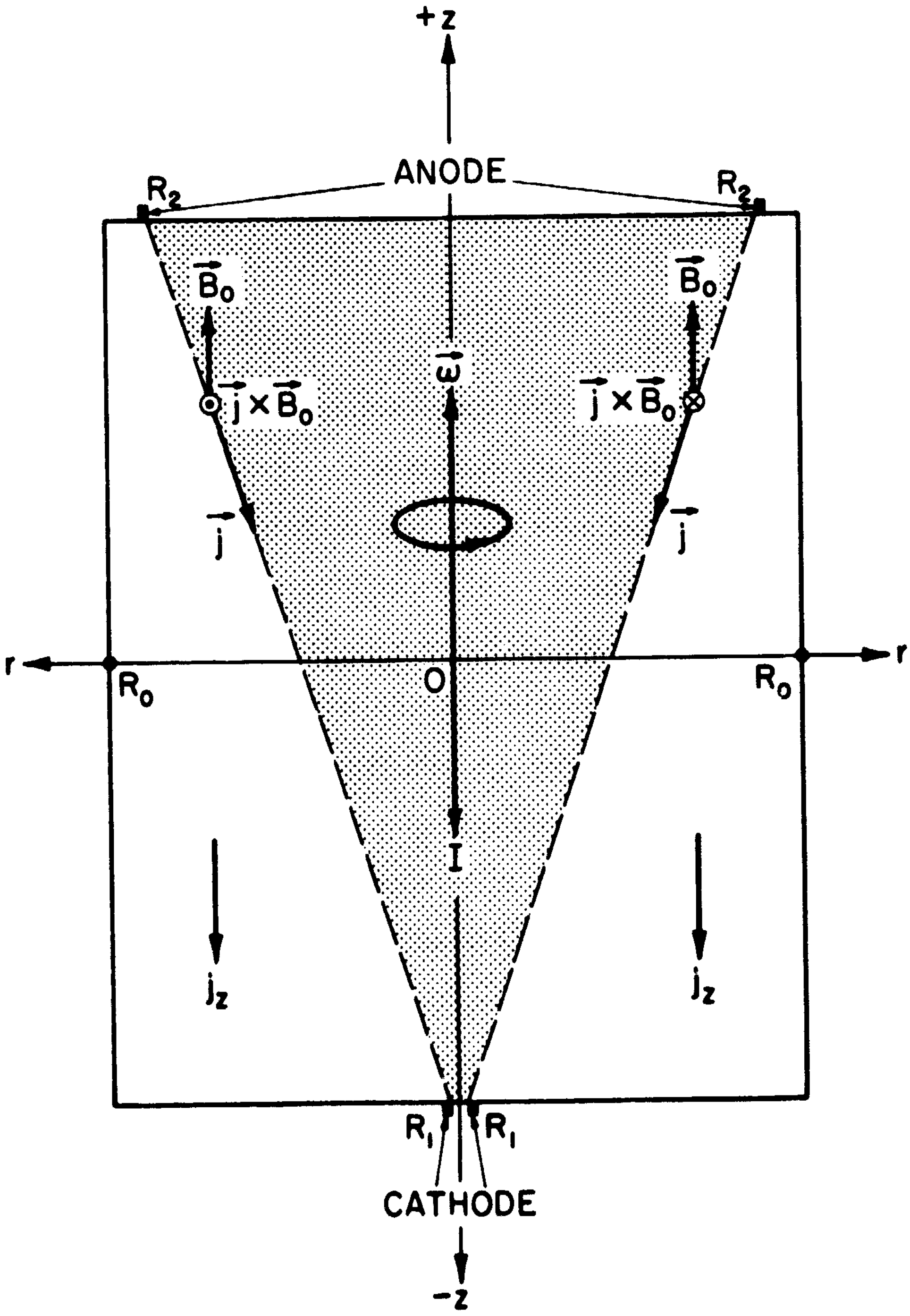

FIG. 0: Geometry of Spatially Diverging Discharge Between Cathode (R_1) and Anode (R_2) in a Cylinder (R_o) with Axial Magnetic Field $\vec{B}_o$ ($R_2 \gg R_1$).

In the ion thruster, the plasma is produced by means of a diffuse, spatially diverging electrical discharge between a hollow cathode of small radius R_1 and a circular anode of considerably larger radius R_2 (at the cylindrical chamber wall).[1)] The field lines of the electric current density $\vec{j}$ and of the confining magnetic field $\vec{B}$ cross under a nonvanishing angle (except at the chamber axis)[2)] so that the resultant Lorentz force $\vec{j} \times \vec{B}$ rotates the discharge around its axis of symmetry. In steady state, the magnetic body forces in azimuthal directions are balanced by viscous forces (boundary layers at the chamber walls). Schematically, this is illustrated in Fig. 0 for a much simpler model of a discharge between a cathode (R_1) and an anode (R_2) in a homogeneous magnetic field $\vec{B}_o$ ($R_2 >> R_1$, rotation in direction $\vec{\omega}$).

In view of the complicated geometry of actual thruster discharges and their inhomogeneous magnetic confinement fields,[1,2)] the steady state rotation of a spatially diverging discharge in an external magnetic field is analyzed by means of the electrical discharge model in a homogeneous axial magnetic field $\vec{B}_o$ depicted in Fig. 0. The analysis is based on the magnetogasdynamic approximation, in which two characteristic nondimensional parameters occur, the Hartman number H and the Hall coefficient $\omega\tau$,

$$H = (\sigma/\mu)^{1/2} B_o R_o , \quad \omega\tau = (|e| B_o/m)\tau \ .$$

The symbols introduced designate the electrical conductivity (σ), the viscosity (μ), the electron gyration frequency (ω), and the electron momentum relaxation time (τ). H and $\omega\tau$ are a measure for the strength of the Lorentz force relative to the viscous friction force and for the reduction of the current flow $\vec{j}_\perp$ transverse to the magnetic field $\vec{B}_o$, respectively. Very little is known about the transport coefficients σ, μ, and τ for low pressure discharges, except the qualitative experimental results that σ is anomalously small, μ is anomalously large, and τ is anomalously small.$^{3)}$

For the above reasons, the dynamics of the rotating discharge in an axial magnetic field will be discussed in terms of the nondimensional parameters H and $\omega\tau$ which are treated as variables within their value domain of practical interest, $H \gtrsim 1$ and $\omega\tau \gtrsim 1$. H and $\omega\tau$ represent phenomenological parameters since σ, μ, and τ have to be obtained by measurements.

THEORETICAL FORMULATION

For a purely azimuthal flow field, $\vec{v} = \{0, v(r,z), 0\}$, the plasma behaves incompressible, $\nabla \cdot \vec{v} = 0$. From the continuity equation, $\nabla \cdot (\rho\vec{v}) = \vec{v} \cdot \nabla\rho = 0$, it follows then that the density gradient $\nabla\rho$ is everywhere perpendicular to the flow field $\vec{v}$. These simple conditions are only approximately realized since the intensity of the secondary flows increases with increasing Reynolds number $R = \bar{\rho}_M \bar{v} R_o/\mu$.4) In absence of secondary flows, momentum cannot be balanced completely in the z-direction, since

$$\partial p/\partial z = 0, \text{ for } \vec{v} = \{0, v(r,z), 0\},$$

in accordance with the z-component of the magnetogasdynamic equation of motion. A strictly z-independent pressure field is physically not possible, since the axial pressure gradient across the boundary layers at the end plates $z = \pm c$ is nonzero, although generally small, $\partial p/\partial z \approx 0$ (boundary-layer approximation for "transverse" pressure gradient).4)

In accordance with the magnetogasdynamic equations,5) Ohm's law with Hall effect,5) and the conservation equation for the electric charge density ($\nabla \cdot \vec{j} = 0$), the rotating discharge in a homogeneous magnetic field $\vec{B}_o$ is described by the following boundary-value problem for the azimuthal velocity $v(r,z)$ and electric potential $\phi(r,z)$ fields (Fig. 0; secondary flows neglected):

$$-\rho_M \frac{v^2}{r} = -\frac{\partial p}{\partial r} + \omega\tau\, \sigma_\perp B_o\left(-\frac{\partial \phi}{\partial r} + v B_o\right) \quad , \qquad (1)$$

$$0 = \mu\left\{\frac{\partial}{\partial r}\left[\frac{1}{r}\frac{\partial}{\partial r}(rv)\right] + \frac{\partial^2 v}{\partial z^2}\right\} - \sigma_\perp B_o\left(-\frac{\partial \phi}{\partial r} + v B_o\right) \quad , \qquad (2)$$

$$\frac{1}{r}\frac{\partial}{\partial r}\left(r \frac{\partial \phi}{\partial r}\right) + \frac{\sigma}{\sigma_\perp}\frac{\partial^2 \phi}{\partial z^2} = B_o \frac{1}{r}\frac{\partial}{\partial r}(r\, v) \quad , \qquad (3)$$

where

$$v(r,z)_{r=R_o} = 0 \ , \quad -c \leq z \leq +c \qquad , \qquad (4)$$

$$v(r,z)_{z=\pm c} = 0 \ , \quad 0 \leq r \leq R_o \qquad , \qquad (5)$$

and

$$-\sigma \, [\partial\phi(r,z)/\partial z]_{z=\pm c} = \quad I \ \delta(r - R_{1,2})/2\pi r \ , \qquad (6)$$

$$[\partial\phi(r,z)/\partial r]_{r=R_o} = 0 \ , \quad -c \leq z \leq +c \qquad . \qquad (7)$$

The boundary conditions (4), (5), and (7) consider that the plasma does not slip at the walls $r = R_o$ and $z = \pm c$, and that no current flows into the cylinder wall $r = R_o$, respectively. The boundary conditions in Eq. (6) imply that the cathode (R_1) and anode (R_2) are ring electrodes of vanishing radial width, $\Delta r \to 0[\delta(r - R_{1,2})/2\pi r =$ radial Dirac function]. The net current flowing through the discharge is by Eq. (6)

$$-2\pi\sigma \int_0^{R_o} \frac{\partial\phi(r,z = \pm c)}{\partial z} \, r dr = I \int_0^{R_o} \delta(r-R_{1,2}) \, dr = I < 0 \quad ,$$

since the positive current (I < 0) flows from the anode to the cathode (Fig. 0). In Eqs. (1) - (3), the transverse conductivity is given by

$$\sigma_\perp = \sigma/(1 + \omega^2\tau^2) \ . \qquad (8)$$

Owing to the disregard of secondary flows, the boundary-value problem is linear since $v(r,z)$ and $\phi(r,z)$ are described by the linear equations (2) - (7). The nonlinear equation (1) determines the pressure field $p(r,z)$ which does not occur in Eqs. (2) - (3). It should be noted that the induced magnetic field has been disregarded under the assumption that the magnetic Reynolds number is small,

$$R_m = \mu_o \sigma_\perp \bar{v} \, R_o \ll 1 \ .$$

ANALYTICAL SOLUTION

The characteristic nondimensional parameters of the magnetogasdynamic discharge problem under consideration are obtained by introducing the nondimensional independent and dependent variables,

$$\rho = r/R_o \ , \quad 0 \leq \rho \leq 1 \qquad , \qquad (9)$$

$$\zeta = z/c \ , \quad -1 \leq \zeta \leq +1 \qquad , \qquad (10)$$

and

$$V(\rho,\zeta) = v(r,z)/v_o , \quad \Phi(\rho,\zeta) = \phi(r,z)/\phi_o \ , \qquad (11)$$

where

$$v_o \equiv \phi_o/R_oB_o \ , \quad \phi_o \equiv Ic/2\pi\sigma R_o^2 \qquad . \qquad (12)$$

In terms of the nondimensional space variables and fields, the boundary-value problem defined in Eqs. (2) - (7) assumes for $V(\rho,\zeta)$ and $\Phi(\rho,\zeta)$ the form:

$$\frac{1}{\rho}\frac{\partial}{\partial\rho}\left(\rho\frac{\partial\Phi}{\partial\rho}\right) + M^{-2}\frac{\partial^2\Phi}{\partial\zeta^2} = \frac{1}{\rho}\frac{\partial}{\partial\rho}(\rho V) \qquad , \qquad (13)$$

$$\frac{\partial}{\partial\rho}\left[\frac{1}{\rho}\frac{\partial}{\partial\rho}(\rho V)\right] + N^{-2}\frac{\partial^2 V}{\partial\zeta^2} - H_\perp^2 V = -H_\perp^2\frac{\partial\Phi}{\partial\rho} \ , \qquad (14)$$

where

$$V(\rho,\zeta)_{\rho=1} = 0 \ , \quad -1 \leq \zeta \leq +1 \qquad , \qquad (15)$$

$$V(\rho,\zeta)_{\zeta=\pm1} = 0 \ , \quad 0 \leq \rho \leq 1 \qquad , \qquad (16)$$

and

$$-[\partial\Phi(\rho,\zeta)/\partial\zeta]_{\zeta=\pm1} = \delta(\rho-\rho_{2,1})/\rho \qquad , \qquad (17)$$

$$[\partial\Phi(\rho,\zeta)/\partial\rho]_{\rho=1} = 0 \qquad , \qquad (18)$$

with $\rho_{2,1} \equiv R_{2,1}/R_o$. The nondimensional constants M, N, and $H_\perp$ are defined by

$$M^{-2} = (1 + \omega^2\tau^2)(R_o/c)^2 \ , \quad N^{-2} = (R_o/c)^2 \ , \tag{19}$$

$$H_\perp^2 = (\sigma_\perp/\mu)B_o^2R_o^2 = H^2/(1 + \omega^2\tau^2) \qquad . \tag{20}$$

In view of the similarity of the left sides of Eqs. (13) - (14) with Bessel's differential equation, $Z_m'' + \rho^{-1}Z_m' + (k_\nu^2 - \rho^{-2}m^2)Z_m = 0$, for cylinder functions $Z_m(k_\nu\rho)$, partial solutions of the coupled inhomogeneous equations are sought in the form,

$$\Phi_\nu(\rho,\zeta) = J_o(k_\nu\rho)f(\zeta) \ , \tag{21}$$

$$V_\nu(\rho,\zeta) = J_1(k_\nu\rho)g(\zeta) \ , \tag{22}$$

where $J_o'(k_\nu\rho) = -J_1(k_\nu\rho)$ and $J_1'(k_\nu\rho) + (k_\nu\rho)^{-1}J_1(k_\nu\rho) = J_o(k_\nu\rho)$. Substitution of Eqs. (21) - (22) into Eqs. (13) - (14) yields

$$\frac{d^2f_\nu}{d\zeta^2} - k_\nu^2\, M^2\, f_\nu = k_\nu\, M^2\, g_\nu \qquad , \tag{23}$$

$$\frac{d^2g_\nu}{d\zeta^2} - (k_\nu^2 + H_\perp^2)N^2g_\nu = k_\nu\, H_\perp^2N^2f_\nu \ , \tag{24}$$

where the eigen-values $k_\nu > 0$ are determined by the boundary conditions (15) and (18) as the real roots of the transcendental equation,

$$J_1(k_\nu) = 0 \ , \quad \nu = 1,2,3,\ldots. \tag{25}$$

Thus, the general solution of the coupled equations (13) - (14) obtains by linear superposition as:

$$\Phi(\rho,\zeta) = \sum_{\nu=1}^{\infty} J_o(k_\nu\rho)f_\nu(\zeta) \ , \tag{26}$$

$$V(\rho,\zeta) = \sum_{\nu=1}^{\infty} J_1(k_\nu\rho)g_\nu(\zeta) \ . \tag{27}$$

By decoupling Eqs. (23) - (24) one finds for $f_\nu(\zeta)$ and $g_\nu(\zeta)$ the differential equations of 4th order,

$$\frac{d^4 f_\nu}{d\zeta^4} - [k_\nu^2(M^2 + N^2) + N^2H_\perp^2]\,\frac{d^2 f_\nu}{d\zeta^2} + f_\nu = 0\ , \tag{28}$$

$$\frac{d^4 g_\nu}{d\zeta^4} - [k_\nu^2(M^2 + N^2) + N^2H_\perp^2]\,\frac{d^2 g_\nu}{d\zeta^2} + g_\nu = 0\ , \tag{29}$$

with

$$-\,[df_\nu(\zeta)/d\zeta]_{\zeta=\pm 1} = 2J_o(k_\nu\rho_{2,1})/J_o(k_\nu)^2\ , \tag{30}$$

$$g(\zeta)_{\zeta=\pm 1} = 0\ , \tag{31}$$

as boundary conditions by Eqs. (16) - (17). In deriving Eq. (30), the Dirac function in Eq. (17) has been expanded,

$$\delta(\rho - \rho_{2,1})/\rho = 2\sum_{\nu=1}^{\infty}[J_o(k_\nu\rho_{2,1})/J_o^2(k_\nu)]J_o(k_\nu\rho)\ . \tag{32}$$

In addition to Eqs (28) - (31), $f_\nu(\zeta)$ and $g_\nu(\zeta)$ have to satisfy also the uncoupled Eqs. (23) - (24). With

$$\omega_{1\nu} \equiv \omega_{\nu+},\ \omega_{2\nu} \equiv \omega_{\nu-},\ \omega_{3\nu} \equiv -\omega_{\nu+},\ \omega_{4\nu} \equiv -\omega_{\nu-}; \tag{33}$$

$$\omega_{\nu\pm} \equiv \Big[\tfrac{1}{2}\{[k_\nu^2(M^2 + N^2) + N^2H_\perp^2] \pm \{[k_\nu^2(M^2 + N^2) + N^2H^2]^2 - 4k_\nu^4M^2N^2\}^{\frac{1}{2}}\}\Big]^{\frac{1}{2}}\ , \tag{34}$$

the general solutions for $f_\nu(\zeta) \sim e^{\omega\zeta}$ and $g_\nu(\zeta) \sim e^{\omega\zeta}$ of Eqs. (28) - (29), can be written as:

$$f_\nu(\zeta) = A_{1\nu}\frac{\sinh\omega_{1\nu}\zeta}{\sinh\omega_{1\nu}} + B_{1\nu}\frac{\cosh\omega_{1\nu}\zeta}{\cosh\omega_{1\nu}} + A_{2\nu}\frac{\sinh\omega_{2\nu}\zeta}{\sinh\omega_{2\nu}} + B_{2\nu}\frac{\cosh\omega_{2\nu}\zeta}{\cosh\omega_{2\nu}}\ , \tag{35}$$

$$g_\nu(\zeta) = C_{1\nu}\frac{\sinh\omega_{1\nu}\zeta}{\sinh\omega_{1\nu}} + D_{1\nu}\frac{\cosh\omega_{1\nu}\zeta}{\cosh\omega_{1\nu}} + C_{2\nu}\frac{\sinh\omega_{2\nu}\zeta}{\sinh\omega_{2\nu}} + D_{2\nu}\frac{\cosh\omega_{2\nu}\zeta}{\cosh\omega_{2\nu}}\ . \tag{36}$$

Only four of the eight integration constants $A_{1\nu}, \ldots, D_{2\nu}$ for any $\nu \geq 1$ are independent; by Eqs (23) - (24),

$$\begin{aligned} (\omega_{1\nu}^2 - k_\nu^2 M^2) A_{1\nu} &= k_\nu M^2 C_{1\nu} \\ (\omega_{2\nu}^2 - k_\nu^2 M^2) A_{2\nu} &= k_\nu M^2 C_{2\nu} \\ (\omega_{1\nu}^2 - k_\nu^2 M^2) B_{1\nu} &= k_\nu M^2 D_{1\nu} \\ (\omega_{2\nu}^2 - k_\nu^2 M^2) B_{2\nu} &= k_\nu M^2 D_{2\nu} \end{aligned} \tag{37}$$

and

$$\begin{aligned} [\omega_{1\nu}^2 - (k_\nu^2 + H_\perp^2) N^2] C_{1\nu} &= k_\nu N^2 H_\perp^2 A_{1\nu} \\ [\omega_{2\nu}^2 - (k_\nu^2 + H_\perp^2) N^2] C_{2\nu} &= k_\nu N^2 H_\perp^2 A_{2\nu} \\ [\omega_{1\nu}^2 - (k_\nu^2 + H_\perp^2) N^2] D_{1\nu} &= k_\nu N^2 H_\perp^2 B_{1\nu} \\ [\omega_{2\nu}^2 - (k_\nu^2 + H_\perp^2) N^2] D_{2\nu} &= k_\nu N^2 H_\perp^2 B_{2\nu} \end{aligned} \tag{38}$$

where the coefficient determinants of the pairs of corresponding equations in Eqs. (37) and (38) vanish owing to Eqs. (33) - (34).

Upon application of the four relations in Eq. (38), which are equivalent to Eq. (37) by Eqs. (33) - (34), and the boundary conditions (31), which give

$$-C_{2\nu} = C_{1\nu} \equiv C_\nu \ , \quad -D_{2\nu} = D_{1\nu} \equiv D_\nu \tag{39}$$

Equations (35) - (36) become:

$$\begin{aligned} f_\nu(\zeta) = {} & \frac{C_\nu}{k_\nu N^2 H_\perp^2} \left\{ \Omega_{1\nu} \frac{\sinh \omega_{1\nu}\zeta}{\sinh \omega_{1\nu}} - \Omega_{2\nu} \frac{\sinh \omega_{2\nu}\zeta}{\sinh \omega_{2\nu}} \right\} \\ & + \frac{D_\nu}{k_\nu N^2 H_\perp^2} \left\{ \Omega_{1\nu} \frac{\cosh \omega_{1\nu}\zeta}{\cosh \omega_{1\nu}} - \Omega_{2\nu} \frac{\cosh \omega_{2\nu}\zeta}{\cosh \omega_{2\nu}} \right\} , \end{aligned} \tag{40}$$

$$g_\nu(\zeta) = C_\nu \left[\frac{\sinh \omega_{1\nu}\zeta}{\sinh \omega_{1\nu}} - \frac{\sinh \omega_{2\nu}\zeta}{\sinh \omega_{2\nu}}\right]$$

$$+ D_\nu \left[\frac{\cosh \omega_{1\nu}\zeta}{\cosh \omega_{1\nu}} - \frac{\cosh \omega_{2\nu}\zeta}{\cosh \omega_{2\nu}}\right] , \tag{41}$$

where

$$\Omega_{i\nu} \equiv \omega_{i\nu}^2 - (k_\nu^2 + H_\perp^2)N^2 \ , \quad i = 1,2 \ . \tag{42}$$

The boundary conditions (30) applied to Eq. (40) yield

$$C_\nu = - \frac{k_\nu N^2 H_\perp^2}{J_o^2(k_\nu)} \ \frac{[J_o(k_\nu\rho_1) + J_o(k_\nu\rho_2)]}{[\omega_{1\nu}\Omega_{1\nu}\mathrm{cth}\omega_{1\nu} - \omega_{2\nu}\Omega_{2\nu}\mathrm{cth}\omega_{2\nu}]} \ , \tag{43}$$

$$D_\nu = + \frac{k_\nu N^2 H_\perp^2}{J_o^2(k_\nu)} \ \frac{[J_o(k_\nu\rho_1) - J_o(k_\nu\rho_2)]}{[\omega_{1\nu}\Omega_{1\nu}\mathrm{tgh}\omega_{1\nu} - \omega_{2\nu}\Omega_{2\nu}\mathrm{tgh}\omega_{2\nu}]} \ . \tag{44}$$

Substitution of Eqs. (43) - (44) into Eqs. (40) - (41) gives as solutions for $f_\nu(\zeta)$ and $g_\nu(\zeta)$:

$$f_\nu(\zeta) \cdot J_o^2(k_\nu) = - \frac{[J_o(k_\nu\rho_1) + J_o(k_\nu\rho_2)]}{[\omega_{1\nu}\Omega_{1\nu}\mathrm{cth}\omega_{1\nu} - \omega_{2\nu}\Omega_{2\nu}\mathrm{cth}\omega_{2\nu}]} \times$$

$$\times \left[\Omega_{1\nu} \frac{\sinh \omega_{1\nu}\zeta}{\sinh \omega_{1\nu}} - \Omega_{2\nu} \frac{\sinh \omega_{2\nu}\zeta}{\sinh \omega_{2\nu}}\right] + \frac{[J_o(k_\nu\rho_1) - J_o(k_\nu\rho_2)]}{[\omega_{1\nu}\Omega_{1\nu}\mathrm{tgh}\omega_{1\nu} - \omega_{2\nu}\Omega_{2\nu}\mathrm{tgh}\omega_{2\nu}]} \times$$

$$\times \left[\Omega_{1\nu} \frac{\cosh \omega_{1\nu}\zeta}{\cosh \omega_{1\nu}} - \Omega_{2\nu} \frac{\cosh \omega_{2\nu}\zeta}{\cosh \omega_{2\nu}}\right] , \tag{45}$$

and

$$g_\nu(\zeta)\cdot\frac{J_o^2(k_\nu)}{k_\nu N^2 H_\perp^2} = -\frac{[J_o(k_\nu\rho_1)+J_o(k_\nu\rho_2)]}{[\omega_{1\nu}\Omega_{1\nu}\mathrm{cth}\omega_{1\nu}-\omega_{2\nu}\Omega_{2\nu}\mathrm{cth}\omega_{2\nu}]}\times$$

$$\times\left[\frac{\sinh\omega_{1\nu}\zeta}{\sinh\omega_{1\nu}}-\frac{\sinh\omega_{2\nu}\zeta}{\sinh\omega_{2\nu}}\right]+\frac{[J_o(k_\nu\rho_1)-J_o(k_\nu\rho_2)]}{[\omega_{1\nu}\Omega_{1\nu}\mathrm{tgh}\omega_{1\nu}-\omega_{2\nu}\Omega_{2\nu}\mathrm{tgh}\omega_{2\nu}]}\times$$

$$\times\left[\frac{\cosh\omega_{1\nu}\zeta}{\cosh\omega_{1\nu}}-\frac{\cosh\omega_{2\nu}\zeta}{\cosh\omega_{2\nu}}\right]. \qquad (46)$$

Equations (45) - (46) form, together with Eqs. (26) - (27), the closed form solution of the problem of the rotating gas discharge in an axial magnetic field $\vec{B}_o$:

$$-\Phi(\rho,\zeta) = \sum_{\nu=1}^{\infty}\frac{J_o(k_\nu\rho)}{J_o^2(k_\nu)}\left\{\frac{[J_o(k_\nu\rho_1)+J_o(k_\nu\rho_2)]}{[\omega_{1\nu}\Omega_{1\nu}\mathrm{cth}\omega_{1\nu}-\omega_{2\nu}\Omega_{2\nu}\mathrm{cth}\omega_{2\nu}]}\times\right.$$

$$\times\left[\Omega_{1\nu}\frac{\sinh\omega_{1\nu}\zeta}{\sinh\omega_{1\nu}}-\Omega_{2\nu}\frac{\sinh\omega_{2\nu}\zeta}{\sinh\omega_{2\nu}}\right]$$

$$\left.-\frac{[J_o(k_\nu\rho_1)-J_o(k_\nu\rho_2)]}{[\omega_{1\nu}\Omega_{1\nu}\mathrm{tgh}\omega_{1\nu}-\omega_{2\nu}\Omega_{2\nu}\mathrm{tgh}\omega_{2\nu}]}\left[\Omega_{1\nu}\frac{\cosh\omega_{1\nu}\zeta}{\cosh\omega_{1\nu}}-\Omega_{2\nu}\frac{\cosh\omega_{2\nu}\zeta}{\cosh\omega_{2\nu}}\right]\right\} \qquad (47)$$

and

$$-V(\rho,\zeta) = N^2H_\perp^2\sum_{\nu=1}^{\infty}\frac{k_\nu J_1(k_\nu\rho)}{J_o^2(k_\nu)}\left\{\frac{[J_o(k_\nu\rho_1)+J_o(k_\nu\rho_2)]}{[\omega_{1\nu}\Omega_{1\nu}\mathrm{cth}\omega_{1\nu}-\omega_{2\nu}\Omega_{2\nu}\mathrm{cth}\omega_{2\nu}]}\times\right.$$

$$\times\left[\frac{\sinh\omega_{1\nu}\zeta}{\sinh\omega_{1\nu}}-\frac{\sinh\omega_{2\nu}\zeta}{\sinh\omega_{2\nu}}\right]$$

$$\left.-\frac{[J_o(k_\nu\rho_1)-J_o(k_\nu\rho_2)]}{[\omega_{1\nu}\Omega_{1\nu}\mathrm{tgh}\omega_{1\nu}-\omega_{2\nu}\Omega_{2\nu}\mathrm{tgh}\omega_{2\nu}]}\left[\frac{\cosh\omega_{1\nu}\zeta}{\cosh\omega_{1\nu}}-\frac{\cosh\omega_{2\nu}\zeta}{\cosh\omega_{2\nu}}\right]\right\}. \qquad (48)$$

The remaining nondimensional discharge fields $\vec{E}^* = -\nabla\phi/E_o$ and $\vec{J} = \vec{J}/J_o$ are given in terms of the solutions for $\Phi(\rho,\zeta)$ and $V(\rho,\zeta)$:

$$E_r^* = -N\,\partial\Phi/\partial\rho\ ,\quad E_\theta^* = 0\ ,\quad E_z^* = -\partial\Phi/\zeta \qquad ,\ (49)$$

$$J_r = N(-\frac{\partial\Phi}{\partial\rho} + V), \quad J_\theta = N\frac{\omega\tau}{1+\omega^2\tau^2}(-\frac{\partial\Phi}{\partial\rho} + V), \quad J_z = -\frac{\partial\Phi}{\partial\zeta} \tag{50}$$

where $E_o = \phi_o/c$, $J_o = \sigma\phi_o/c$, and $N = c/R_o$ [Eq. (12)].

If the cathode is in the plane $z = -c$ ($\zeta = -1$) and the anode is in the plane $z = +c$ ($\zeta = +1$), then the reference fields v_o and ϕ_o [Eq. (12)] are negative, since $I<0$. The results are also applicable to the case where the anode is in the plane $z = -c$ ($\zeta = -1$) and the cathode is in the plane $z = +c$ ($\zeta = +1$). In the latter situation, the reference fields v_o and ϕ_o [Eq. (12)] are positive, since $I>0$. These explanations hold for magnetic fields pointing in the positive z- direction, $B_o>0$; v_o changes its sign if $B_o<0$ [Eq. (12)].

NUMERICAL ILLUSTRATIONS

As an illustration, the radial (ρ) dependence of the nondimensional discharge fields $V(\rho,\zeta)$, $\Phi(\rho,\zeta)$, $E_r(\rho,\zeta)$, $E_z(\rho,\zeta)$, and $J_r(\rho,\zeta)$ has been calculated for $I < 0$ in the cross sectional planes $\zeta = -0.9$ (cathode region), $\zeta = 0$ (central region), and $\zeta = +0.9$ (anode region) based on Eqs. (47)-(50). The remaining fields $J_\theta(\rho,\zeta)$ and $J_z(\rho,\zeta)$ are simply proportional to $J_r(\rho,\zeta)$ and $E_z(\rho,\zeta)$, respectively [Eq. (50)]. The characteristic (nondimensional) magnetic interaction numbers are treated as parameters:

$$\omega\tau = 1,\ 10,\ 100; \qquad H = 1,\ 10,\ 100.$$

The geometry parameter N is taken to be $N = 1$ so that $M^{-2} = 1 + \omega^2\tau^2$, corresponding to $R_o = c$ [Eq. (20)]. The radial positions of the cathode and anode are assumed to be:

$$\rho_1 = 0.01\ (R_1 = 0.01\ R_o) \quad ; \quad \rho_2 = 0.9\ (R_2 = 0.9\ R_o) \quad .$$

The dimensional fields are negative everywhere where the nondimensional fields are positive, and vice-versa [Eq. (11)] since $v_o < 0$ and $\phi_o < 0$ for $I < 0$ [Eq. (12)].

Central Region, $\zeta = 0$: In Figs. 1-9, the potential Φ, the radial electric field E_r, and the azimuthal flow field V are represented versus ρ for $\zeta = 0$ and $\omega\tau = 1, 10, 100$; $H = 1, 10, 100$. The extrema of V and E_r^* move towards the center $\rho = 0$ as $\omega\tau$ and/or H are increased. Φ always decreases from a maximum at $\rho = 0$ to a minimum at $\rho = 1$ [$E_r(\rho = 1, \zeta) = 0$]. It is remarkable that at certain values of $\omega\tau$ and H the fields Φ, E_r and V exhibit an "oscillatory" radial distribution ($E_r \gtrless 0$, $V \leq 0$; the oscillation amplitudes of Φ are generally too small to be visible in the Φ curves).

The Figs. 10-12 show the axial electric field E_z versus ρ for $\zeta = 0$ and $\omega\tau = 1, 10, 100$; $H = 1, 10, 100$. It is seen that E_z is particularly strong in the center, $\rho \cong 0$, and changes repeatedly its sign at larger ρ values, e.g. in an oscillatory manner for larger $\omega\tau$ and/or H values. This means that the bulk axial current flows in a narrow region, $\rho \cong 0$, in the direction anode→cathode, outside of which the axial current density J_z changes periodically its sign. The pronounced maximum of E_z at $\rho \cong 0.9$, is due to the effect of the anode at $\rho = 0.9$, $\zeta = +1$ on E_z in the plane $\zeta = 0$.

The Figs. 13-15 represent the radial current density J_r versus ρ for $\zeta = 0$ and $\omega\tau = 1, 10, 100$; $K = 1, 10, 100$. J_r vanishes always for $\rho = 0$ (symmetry) and $\rho = 1$ [$J_r(\rho = 1, \zeta) = 0$]. The bulk of the radial current flows in a restricted radial region off the center $\rho = 0$ ($\zeta = 0$!). The extremum of J_r at $\rho \cong 0.85$ reflects the influence of the anode at $\rho = 0.9$, $\zeta = +1$ on J_r in the plane $\zeta = 0$. At sufficiently large values of $\omega\tau$ and/or H, J_r flows periodically forward and back radially in accordance with the oscillatory radial structures of E_r and the induced electric field $- V$.

Cathode Region, $\zeta = -0.9$: In Figs. 16-24, the fields Φ, E_r, and V are shown versus ρ for $\zeta = -0.9$ and $\omega\tau = 1, 10, 100$; $H = 1, 10, 100$, which exhibit a radial structure qualitatively similar to that of the corresponding fields in the plane $\zeta = 0$. - The Figs. 25-27 show E_z versus ρ for $\zeta = -0.9$ and $\omega\tau = 1, 10, 100$; $H = 1, 10, 100$, which is qualitatively similar to E_z in the plane $\zeta = 0$. The Figs. 28-30 show J_r versus ρ for $\zeta = -0.9$ and $\omega\tau = 1, 10, 100$; $H = 1, 10, 100$, which is qualitatively similar to J_r in the plane $\zeta = 0$. - These comparisons indicate that the bulk discharge remains concentrated around the axis $\rho = 0$ from the cathode region $\zeta \cong -0.9$ to the central region $\zeta \cong 0$. It is remarkable that the discharge does not spread significantly in radial direction with increasing axial distance ζ within the interval $-0.9 \leq \zeta \leq 0$ although the ratio of anode and cathode radii is $\rho_2/\rho_1 = R_2/R_1 = 90$.

Anode Region, $\zeta = +0.9$: In Figs. 31-39, Φ, E_r, and V are represented versus ρ for $\zeta = +0.9$ and $\omega\tau = 1, 10, 100$; $H = 1, 10, 100$. One recognizes that the discharge has spread radially, in particular at moderate values of $\omega\tau$ and H, in the plane $\zeta = +0.9$ due to the influence of the anode at $\rho = 0.9$ and $\zeta = +1$. - The Figs. 40-42 show E_z versus ρ for $\zeta = +0.9$ and $\omega\tau = 1, 10, 100$; $H = 1, 10, 100$. For moderate values of $\omega\tau$ and H, E_z is strongest at $\rho \doteq 0.9$, whereas E_z is strongest at $\rho \doteq 0$ for large values of $\omega\tau$ and/or H. - The Figs. 43-45 show J_r versus ρ for $\zeta = +0.9$ and $\omega\tau = 1, 10, 100$; $H = 1, 10, 100$. J_r is most intense i) at $\rho \doteq 0.9$ for moderate values of $\omega\tau$ and H and ii) at $\rho \doteq 0$ for large values of $\omega\tau$ and/or H. - It is evident that the axial magnetic field inhibits the radial spreading of the discharge at sufficiently large values of $\omega\tau$ and/or H. The discharge bends around toward the circular anode of radius $\rho_2 \gg \rho_1$ in a thin layer $\Delta\zeta$ close to the anode plane $\zeta = +1$, where $\Delta\zeta$ is the smaller the larger $\omega\tau$ and/or H are.

The above results are readily applicable to ordinary dense discharges with known transport properties. An application of the theory presented to the thruster discharge is more difficult, since the "anomalous" transport properties (μ, σ, τ) of low density discharge plasmas are not known. Other complications arise from the presence of the baffle electrode, which bisects the discharge region, and the inhomogeneity of the external magnetic field. With some confidence, however, the following qualitative conclusions should hold:

The torque produced by the Lorentz forces rotates the thruster discharge around the chamber axis. For $|I| = 1$ amp, $B_o = 10^{-2}$ Tesla, $\sigma = 10^4$ mho m^{-1}, $R_o = c = 10^{-1}m$, one has $O[v_o] = 10^{-1}m\ sec^{-1}$ and, hence, by Fig. 6, $O[V] = 10^4 m\ sec^{-1}$ for $\omega\tau = 10$, $H = 10^2$.

The usual assumption of an approximately homogeneous current distribution throughout the discharge space is most probably inapplicable. It must rather be assumed that the discharge current is concentrated in a narrow region around the chamber axis and a thin layer on the cathode side of the baffle. In the annular gap surrounding the baffle, the current density should be extremely high and restricted to a thin layer adjacent to the baffle.

Conductivity estimates based on the assumption of a homogeneous current density in the annular gap between the baffle and the cylinder piece will necessarily be too pessimistic. The radial spreading of the thruster discharge is considerably reduced by the magnetic confinement field at Hall coefficients $\omega\tau >> 1$.

REFERENCES

1. H.R. Kaufman, NASA TN-D-585 (1961). W.R. Kerslake and E.V. Pawlik, NASA TN-D-1411 (1963).

2. R.C. Finke, NASA TMX-71612. P.J. Wilbur, NASA CR-134532 (1973).

3. I. Merrill and L. Webb, Phys. Rev. 55, 1171 (1931). O. Buneman, Phys. Rev. 113, 383 (1959).

4. H. Schlichting, Boundary Layer Theory, McGraw-Hill, New York, 1960.

5. L.E. Kalikhman, Magnetogasdynamics, W.B. Saunders, Philadelphia, 1967.

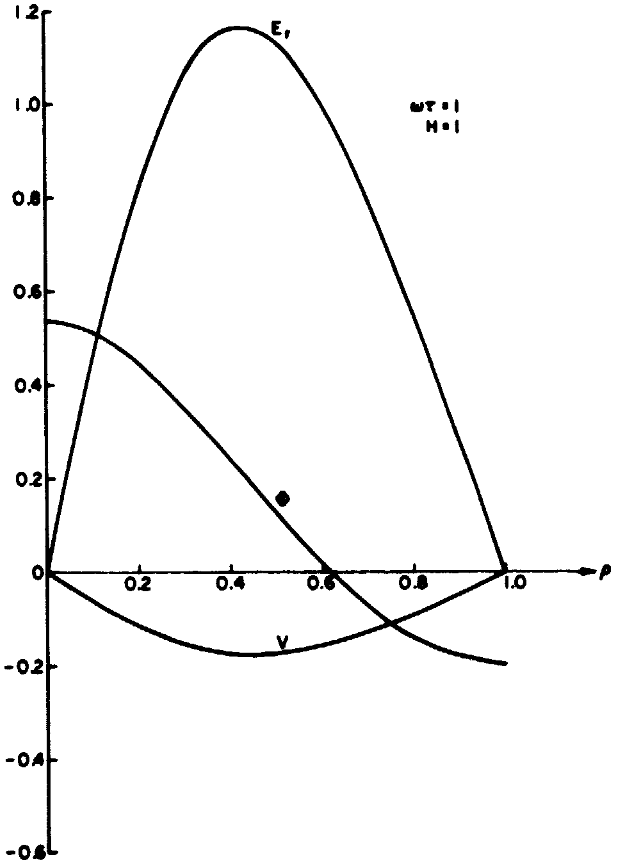

FIG. 1: Φ, E_r, and V versus ρ for $\zeta = 0$, and $\omega\tau = 1$; $H = 1$.

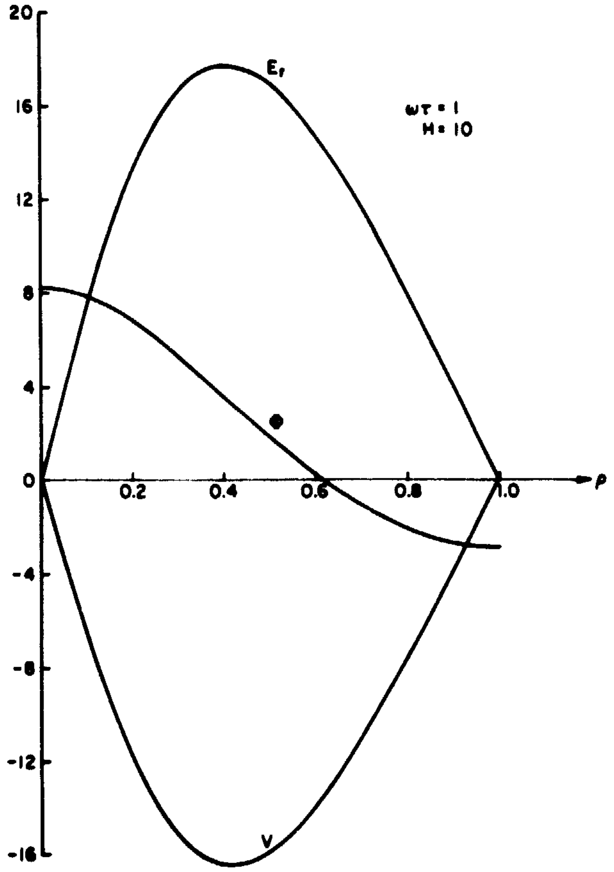

FIG. 2: Φ, E_r, and V versus ρ for $\zeta = 0$, and $\omega\tau = 1$; H = 10.

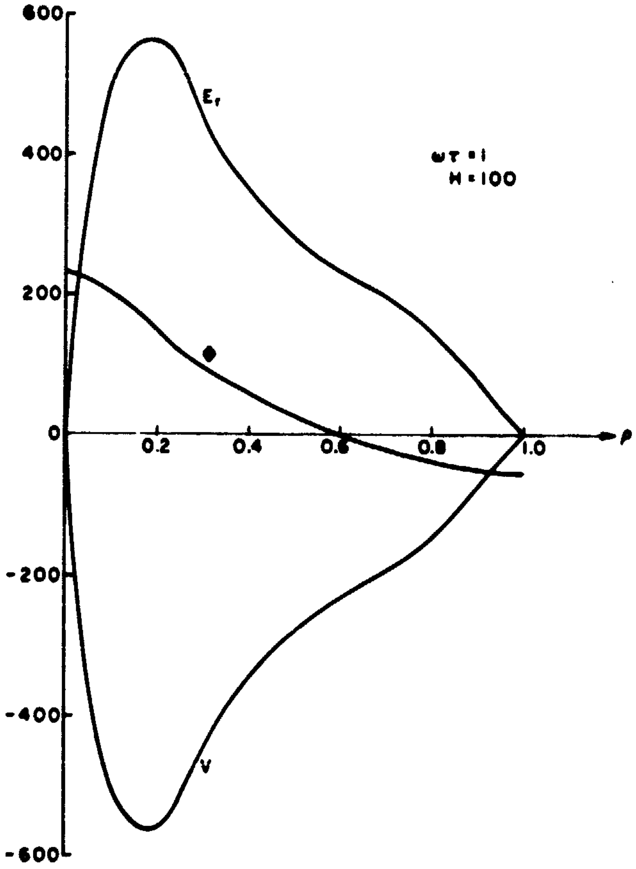

FIG. 3: Φ, E_r, and V versus ρ for $\zeta = 0$, and $\omega\tau = 1$; H = 100.

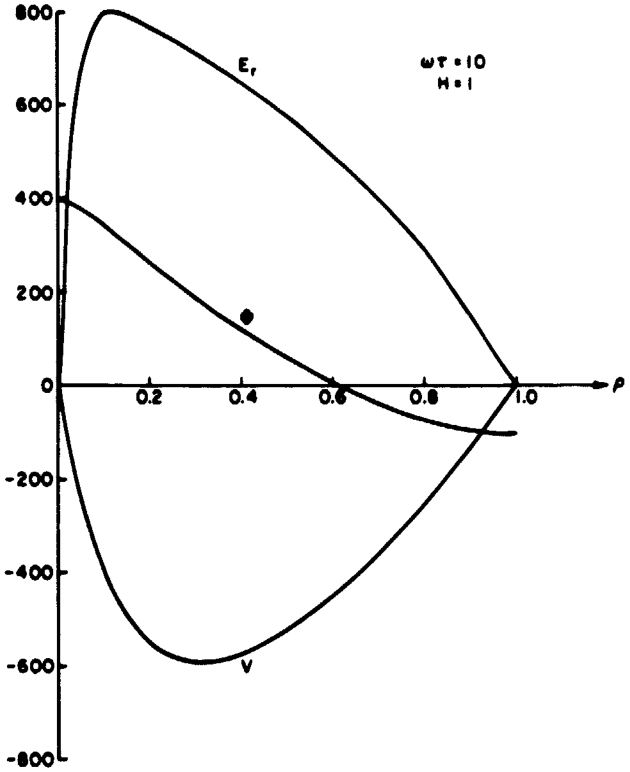

FIG. 4: Φ, E_r, and V versus ρ for ζ = 0, and ωτ = 10; H = 1.

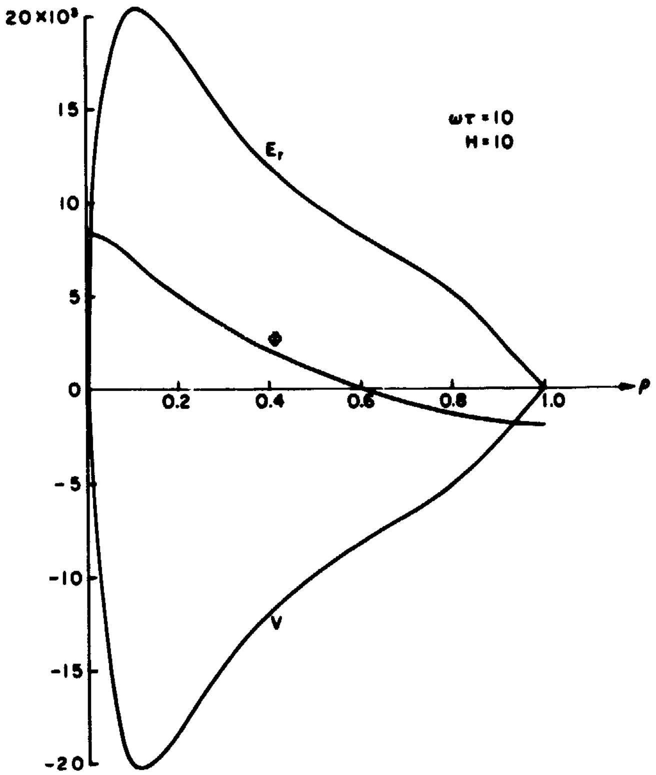

FIG. 5: Φ, E_r, and V versus ρ for $\zeta = 0$, and $\omega\tau = 10$; $H = 10$.

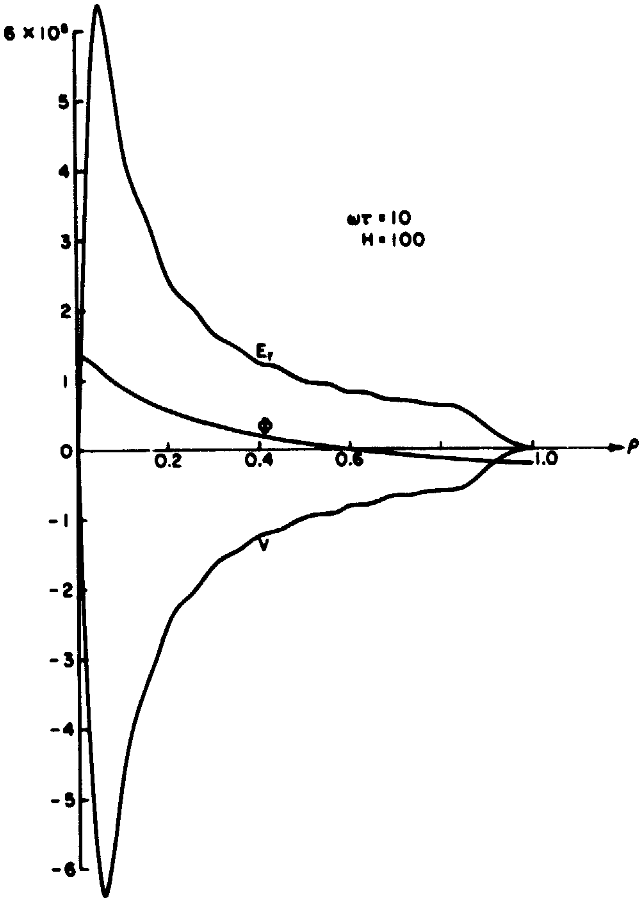

FIG. 6: Φ, E_r, and V versus ρ for $\zeta = 0$, and $\omega\tau = 10$; $H = 100$.

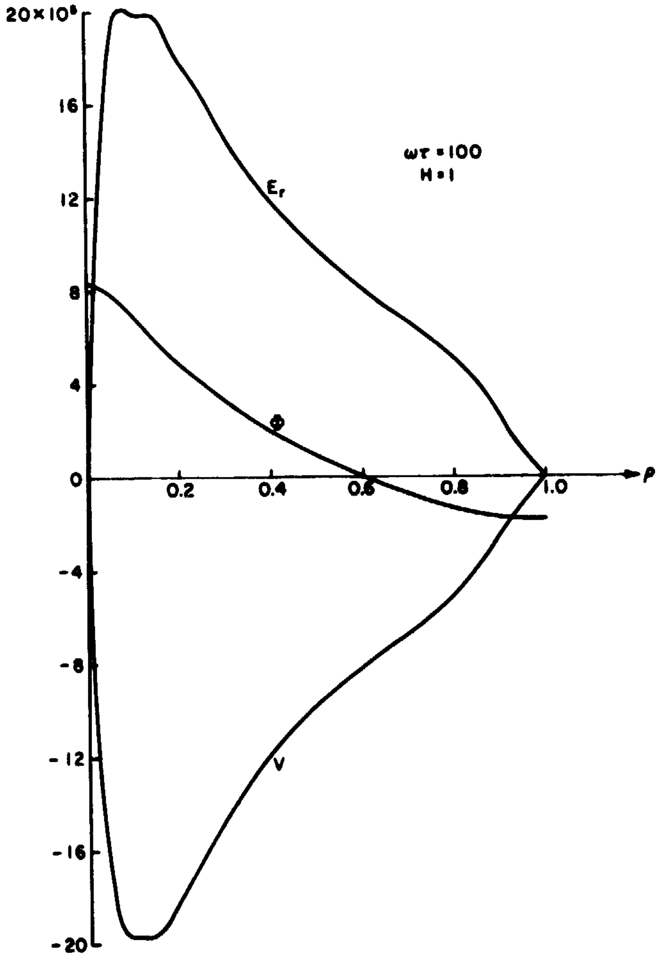

FIG. 7: Φ, E_r, and V versus ρ for $\zeta = 0$, and $\omega\tau = 100$; $H = 1$.

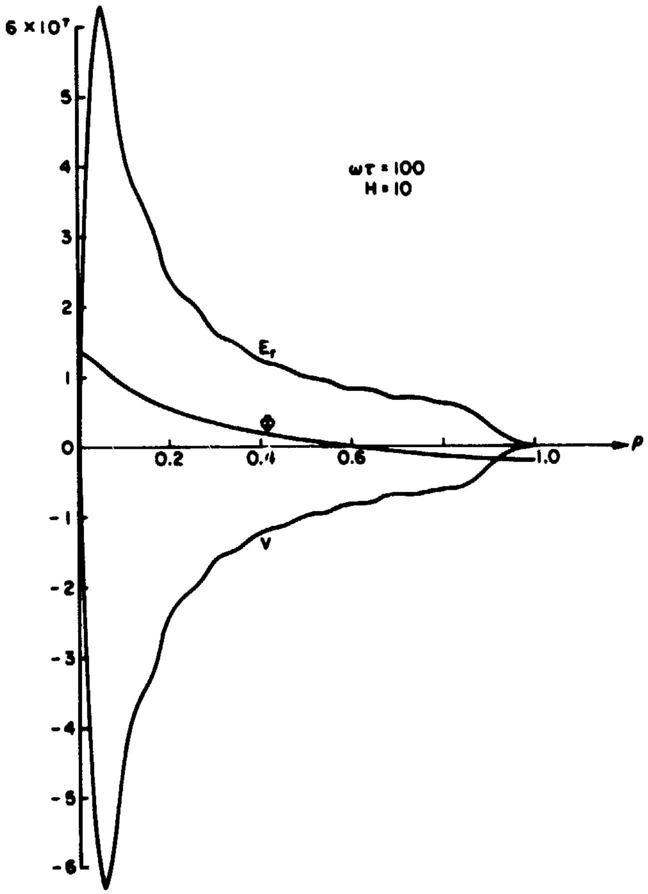

FIG. 8: Φ, E_r, and V versus ρ for $\zeta = 0$, and $\omega\tau = 100$; $H = 10$.

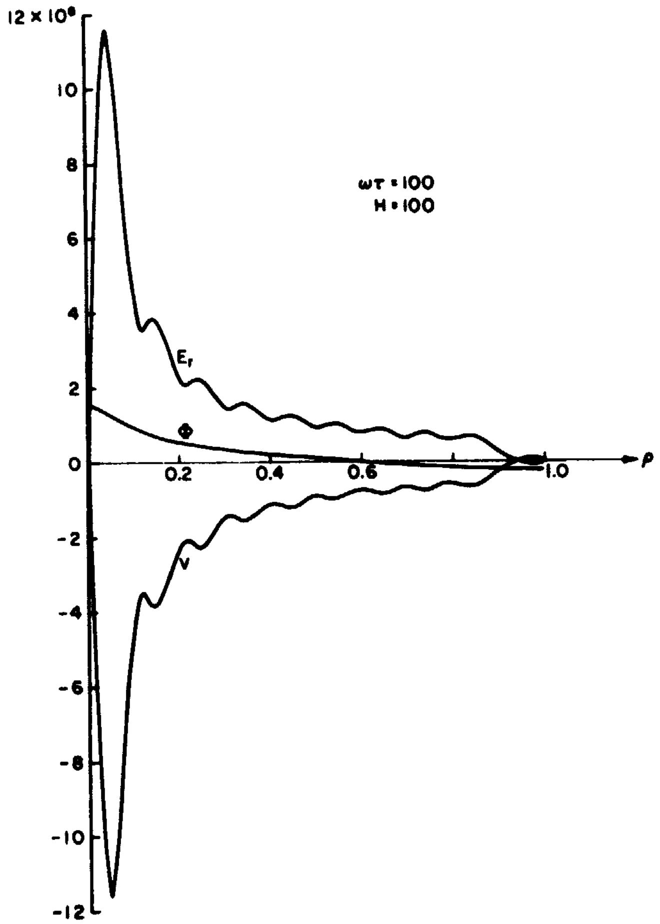

FIG. 9: Φ, E_r, and V versus ρ for $\zeta = 0$, and $\omega\tau = 100$; $H = 100$.

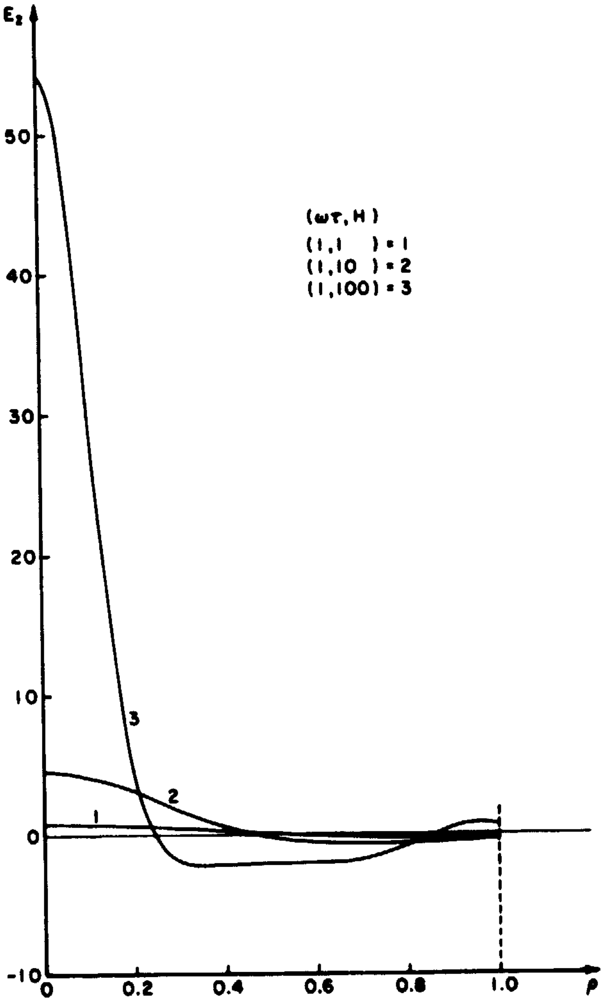

FIG. 10: E_z versus ρ for $\zeta = 0$, and $\omega\tau = 1$; $H = 1, 10, 100$.

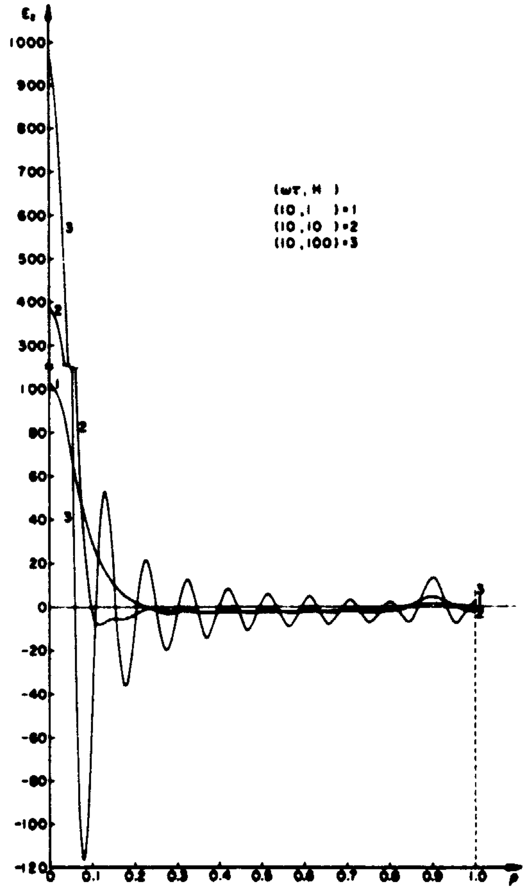

FIG. 11: E_z versus ρ for $\zeta = 0$, and $\omega\tau = 10$; $H = 1, 10, 100$.

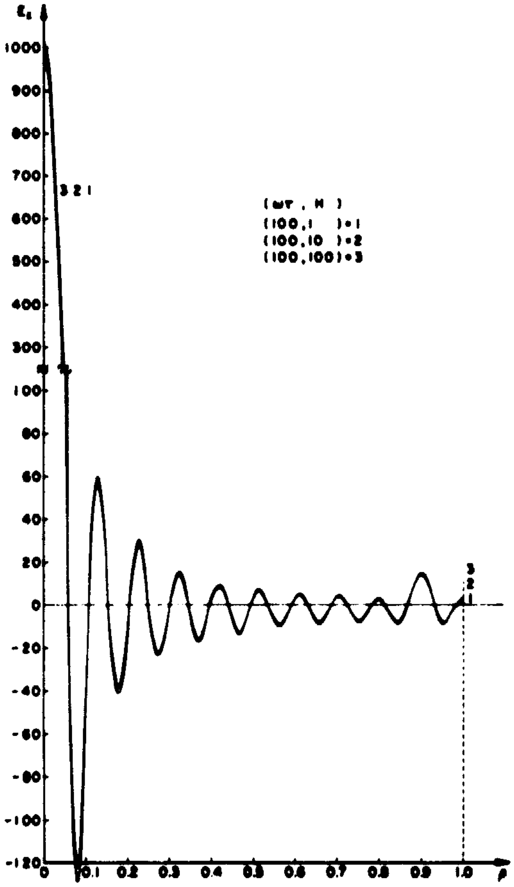

FIG. 12: E_z versus ρ for $\zeta = 0$, and $\omega\tau = 100$;
$H = 1, 10, 100$.

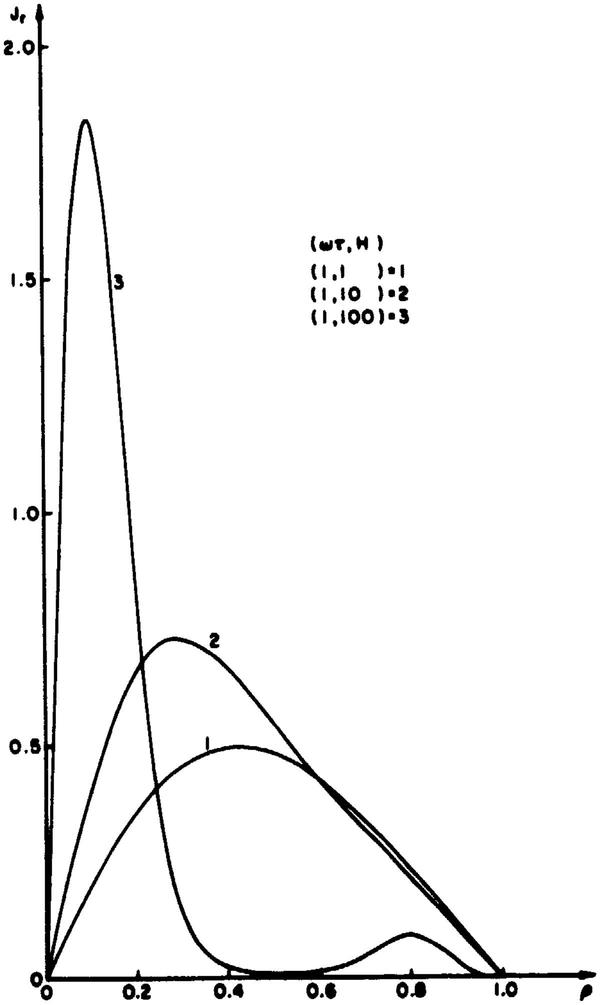

FIG. 13: J_r versus ρ for $\zeta = 0$, and $\omega\tau = 1$; $H = 1, 10, 100$.

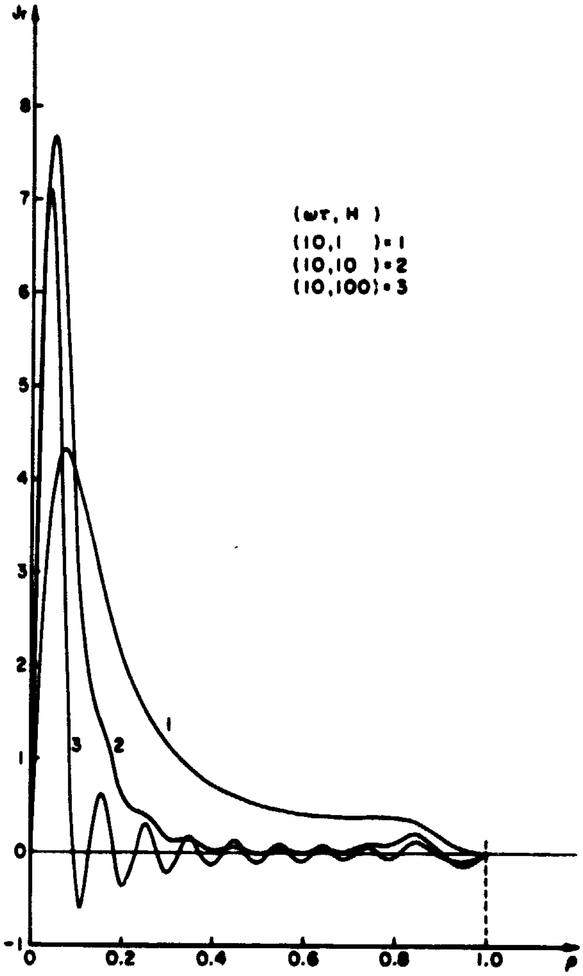

FIG. 14: J_r versus ρ for $\zeta = 0$, and $\omega\tau = 10$; $H = 1, 10, 100$.

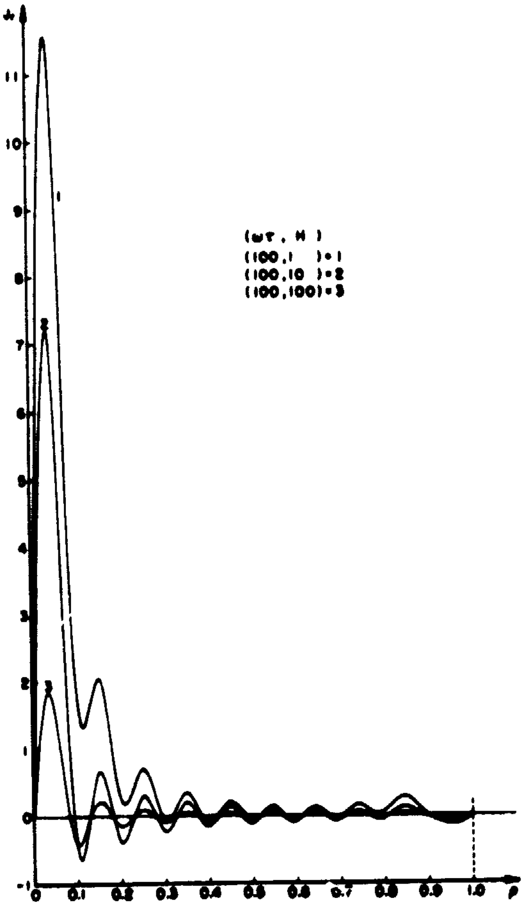

FIG. 15: J_r versus ρ for $\zeta = 0$, and $\omega\tau = 100$; $H = 1, 10, 100$.

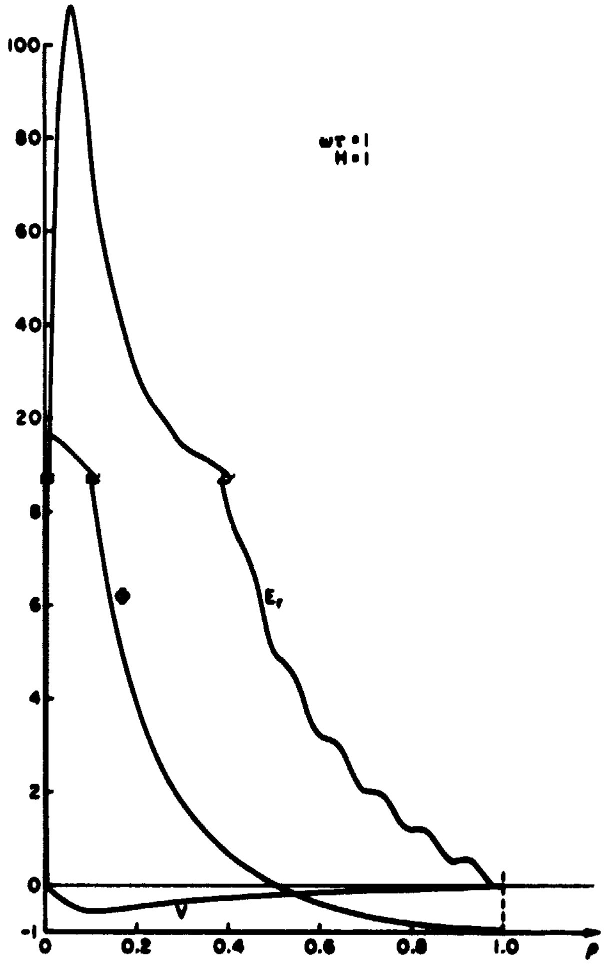

FIG. 16: Φ, E_r, and V versus ρ for ζ = −0.9, and ωτ = 1; H = 1.

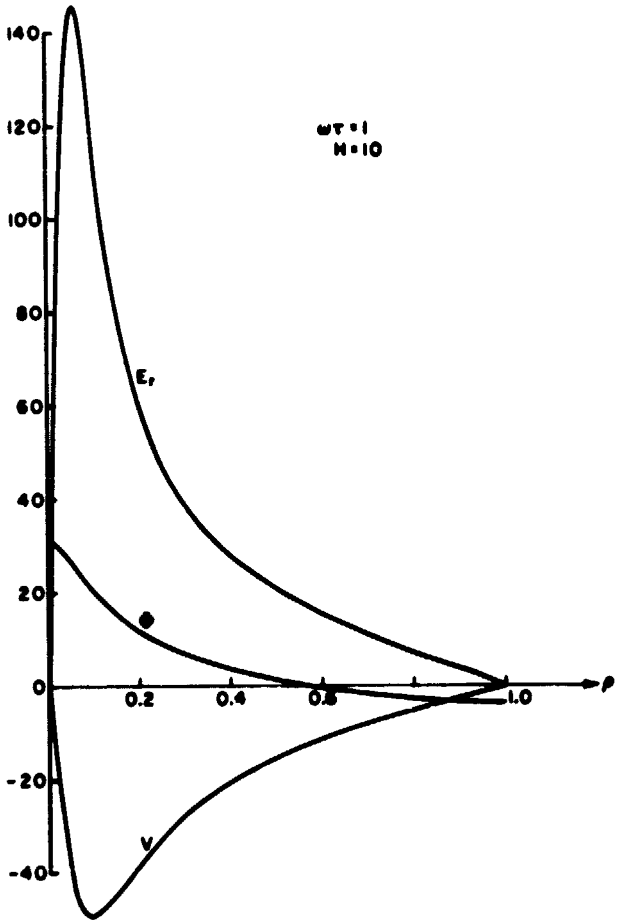

FIG. 17: Φ, E_r, and V versus ρ for ζ = −0.9, and ωτ = 1; H = 10.

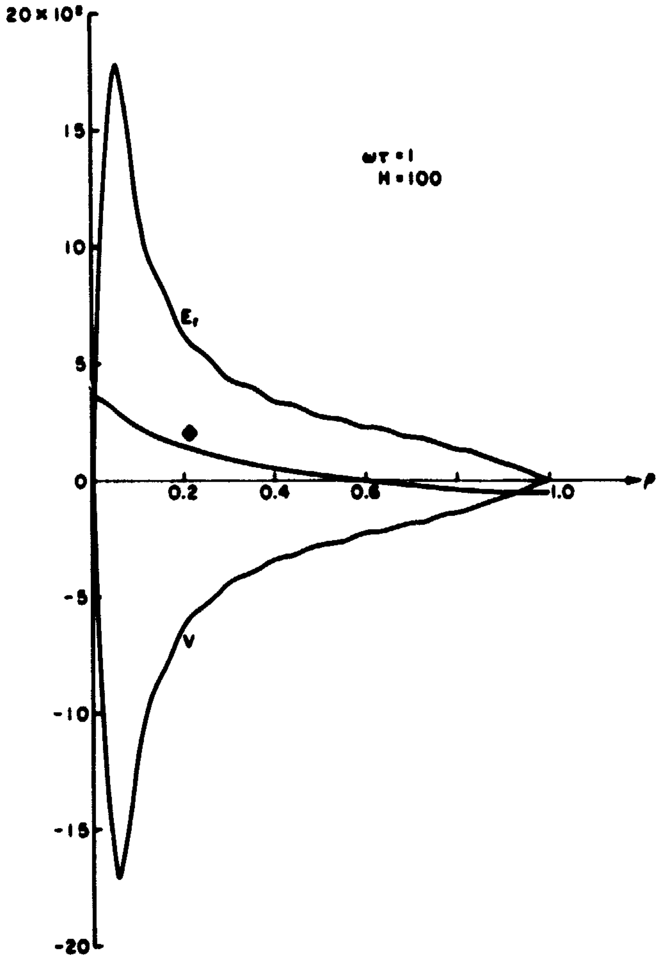

FIG. 18: Φ, E_r, and V versus ρ for $\zeta = -0.9$, and $\omega\tau = 1$, $H = 100$.

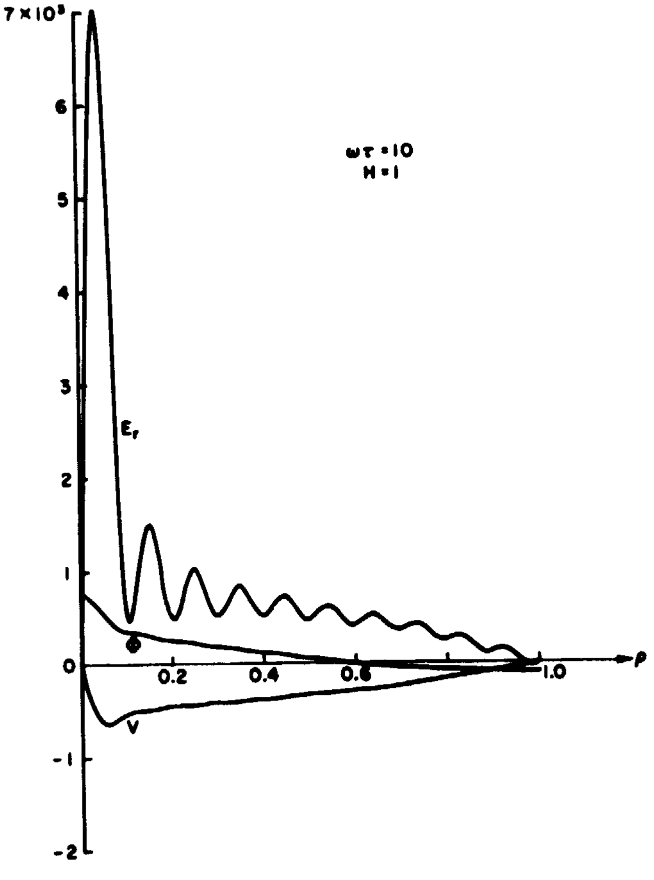

FIG. 19: Φ, E_r, and V versus ρ for ζ = -0.9, and ωτ = 10; H = 1.

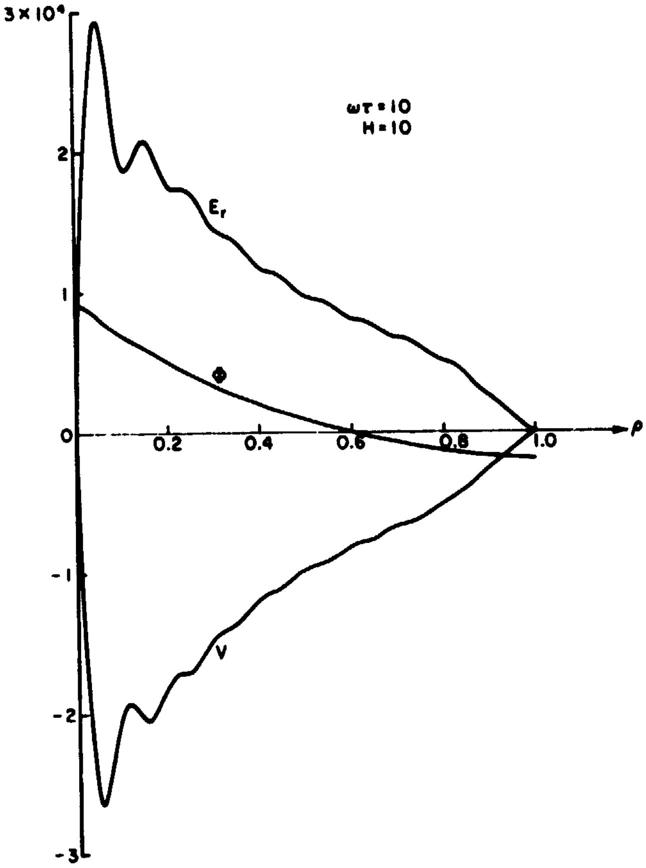

FIG. 20: Φ, E_r, and V versus ρ for $\zeta = -0.9$, and $\omega\tau = 10$; H = 10.

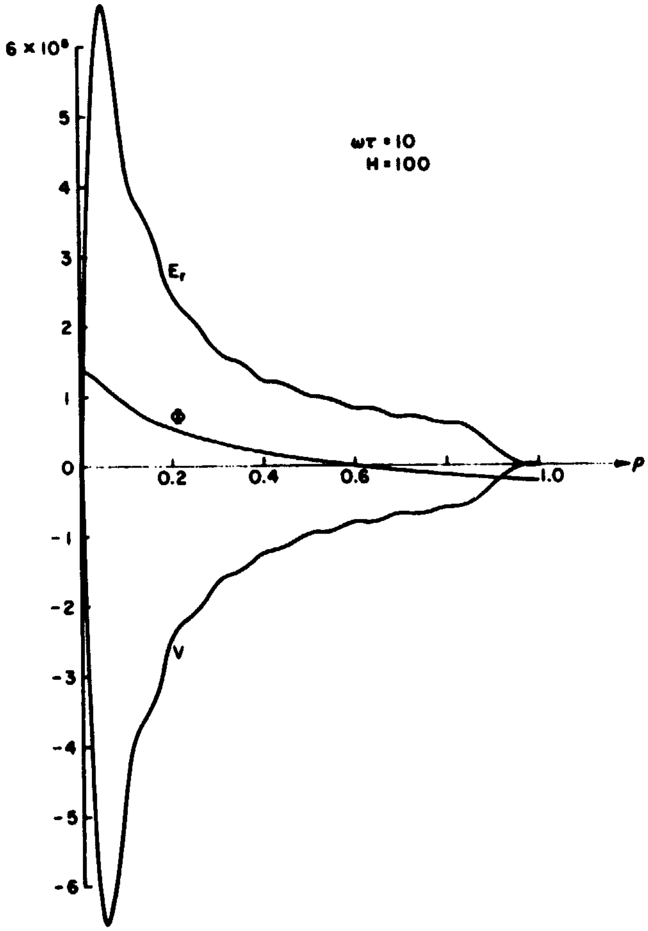

FIG. 21: Φ, E_r, and V versus ρ for $\zeta = -0.9$, and $\omega\tau = 10$; $H = 100$.

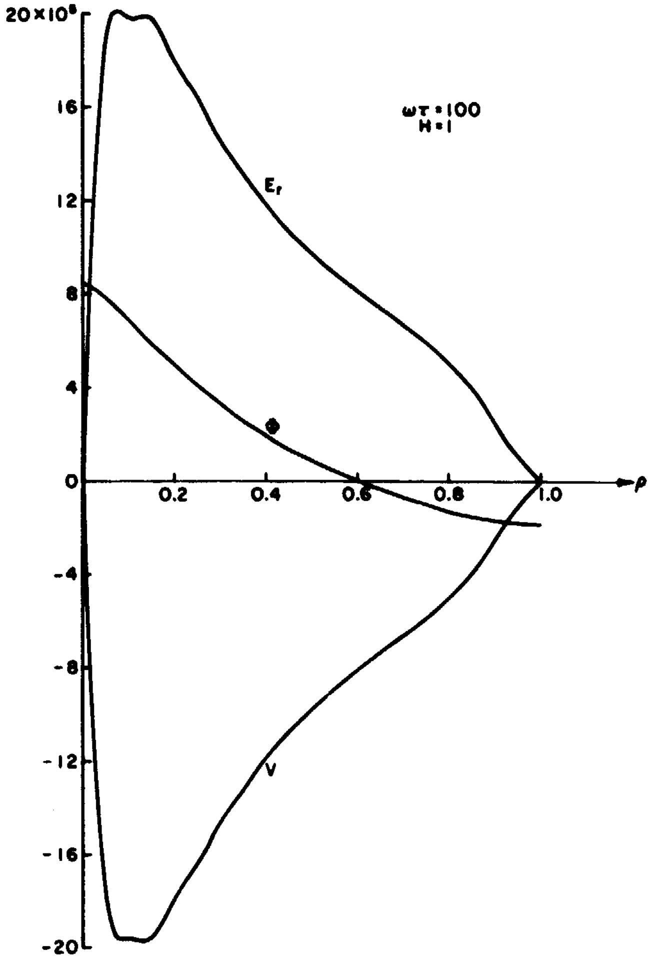

FIG. 22: Φ, E_r, and V versus ρ for $\zeta = -0.9$, and $\omega\tau = 100$; $H = 1$.

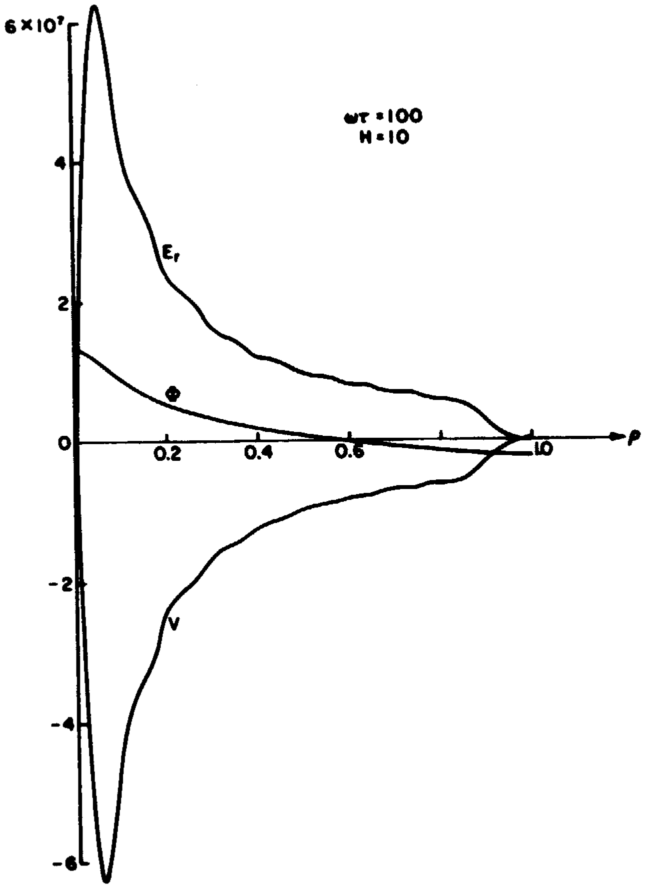

FIG. 23: Φ, E_r, and V versus ρ for $\zeta = -0.9$, and $\omega\tau = 100$; H = 10.

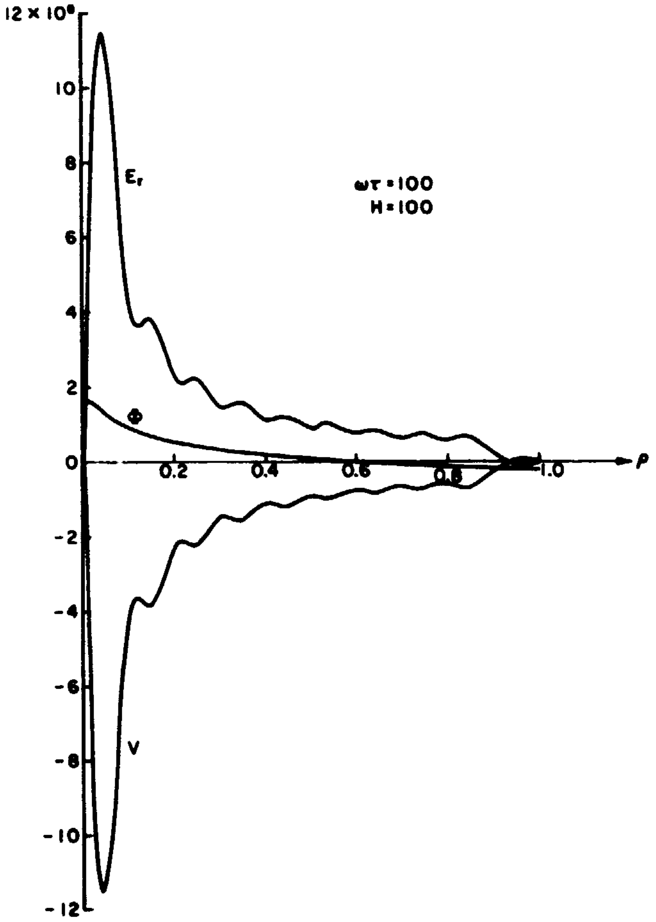

FIG. 24: Φ, E_r, and V versus ρ for $\zeta = -0.9$, and $\omega\tau = 100$; $H = 100$.

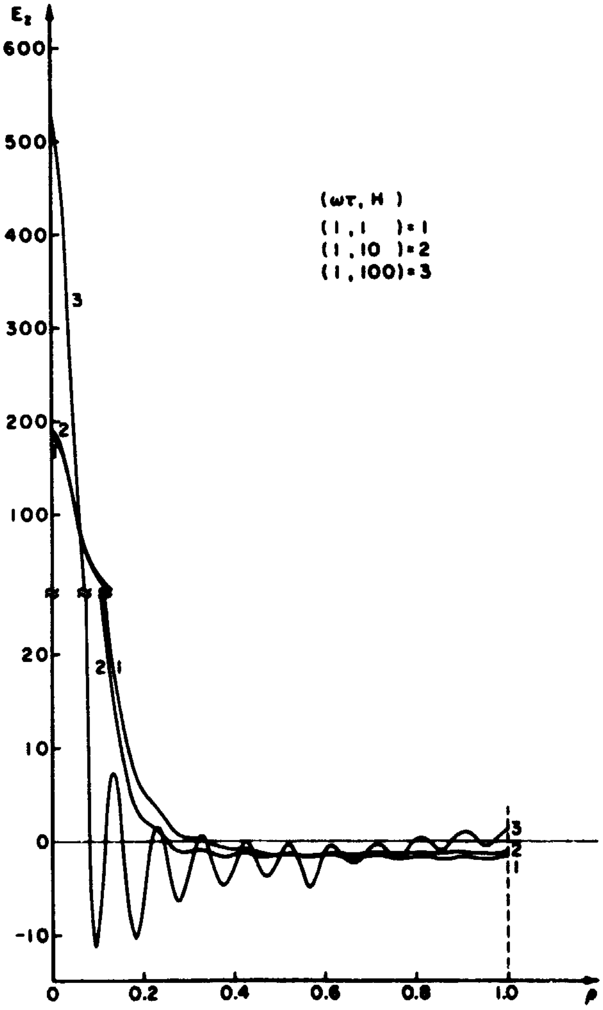

FIG. 25: E_z versus ρ for $\zeta = -0.9$, and $\omega\tau = 1$; $H = 1, 10, 100$.

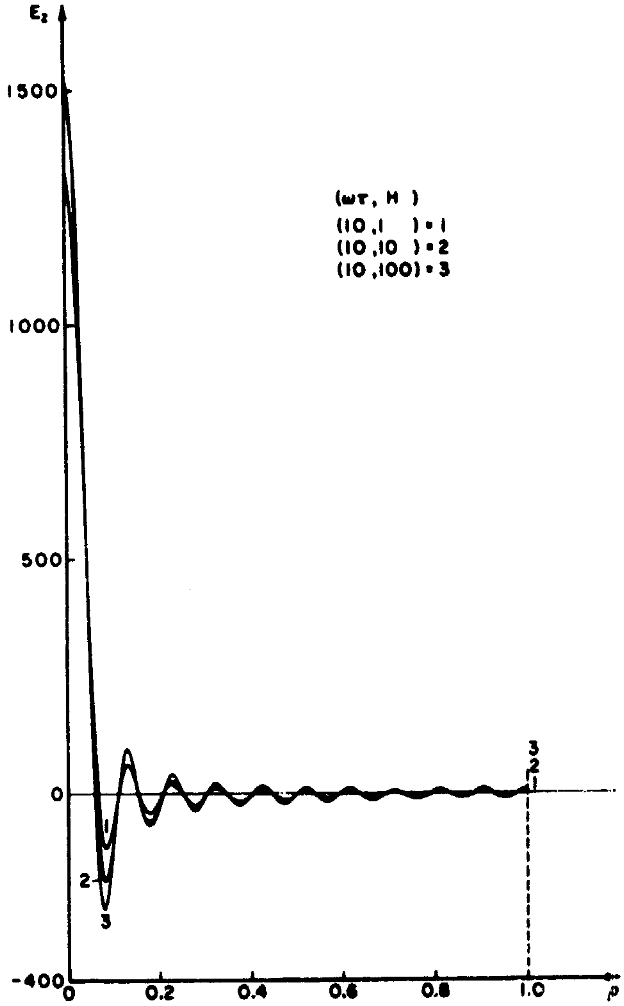

FIG. 26: E_z versus ρ for $\zeta = -0.9$, and $\omega\tau = 10$; $H = 1, 10, 100$.

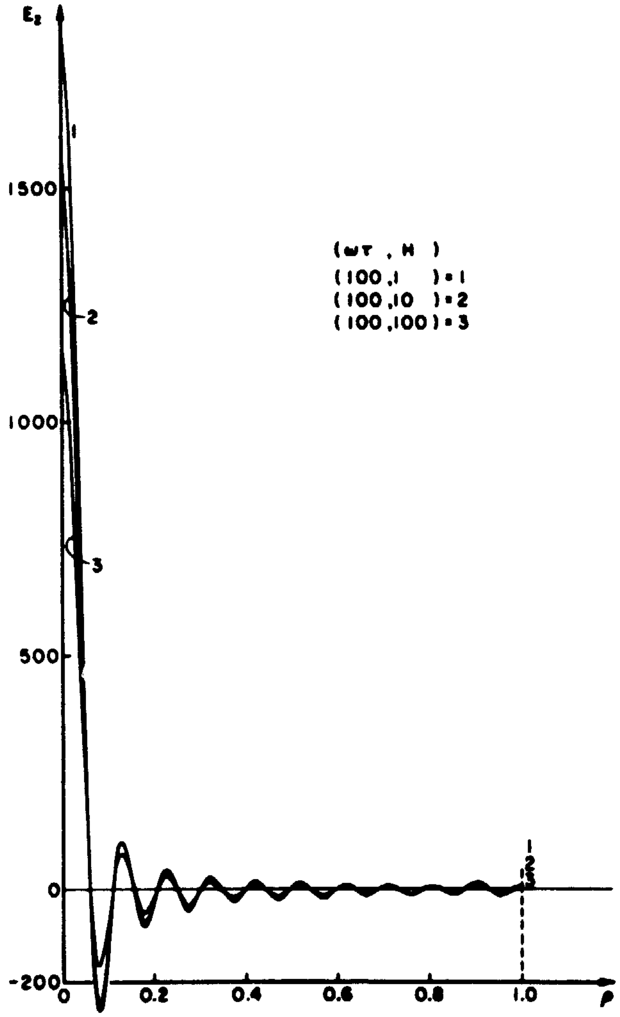

FIG. 27: E_z versus ρ for $\zeta = -0.9$, and $\omega\tau = 100$; $H = 1, 10, 100$.

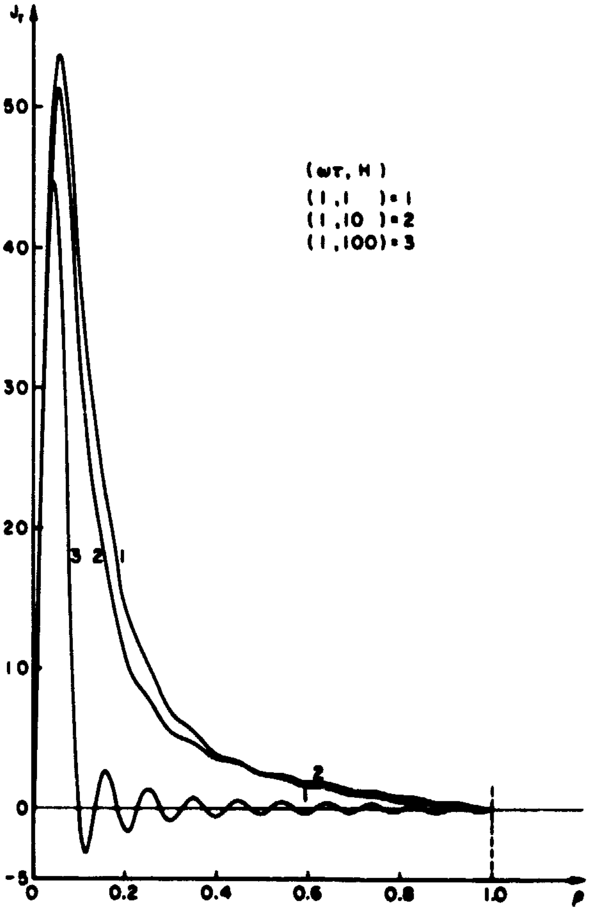

FIG. 28: J_r versus ρ for $\zeta = -0.9$, and $\omega\tau = 1$; $H = 1, 10, 100$.

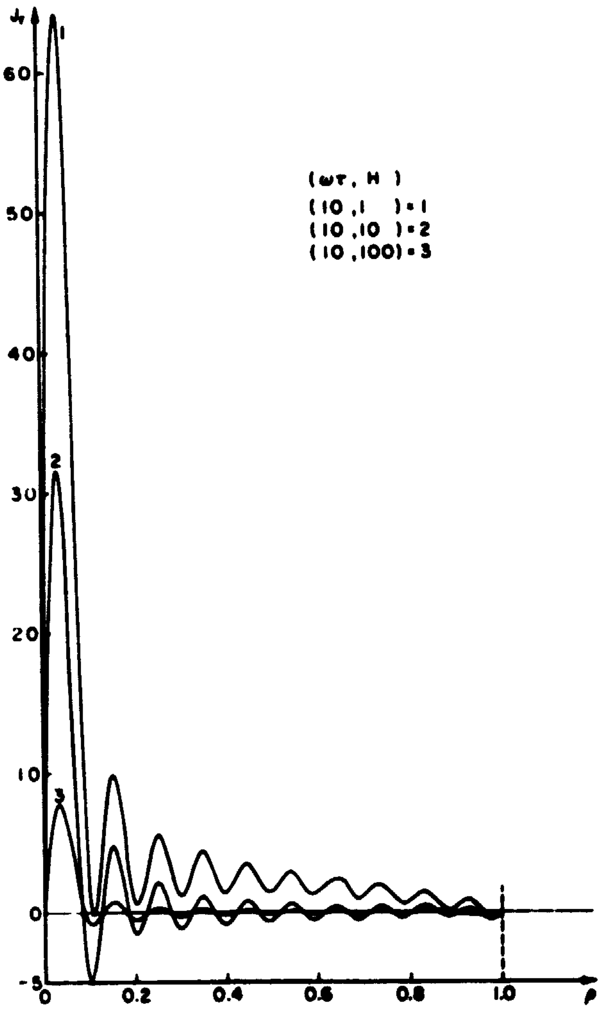

FIG. 29: J_r versus ρ for $\zeta = -0.9$, and $\omega\tau = 10$; $H = 1, 10, 100$.

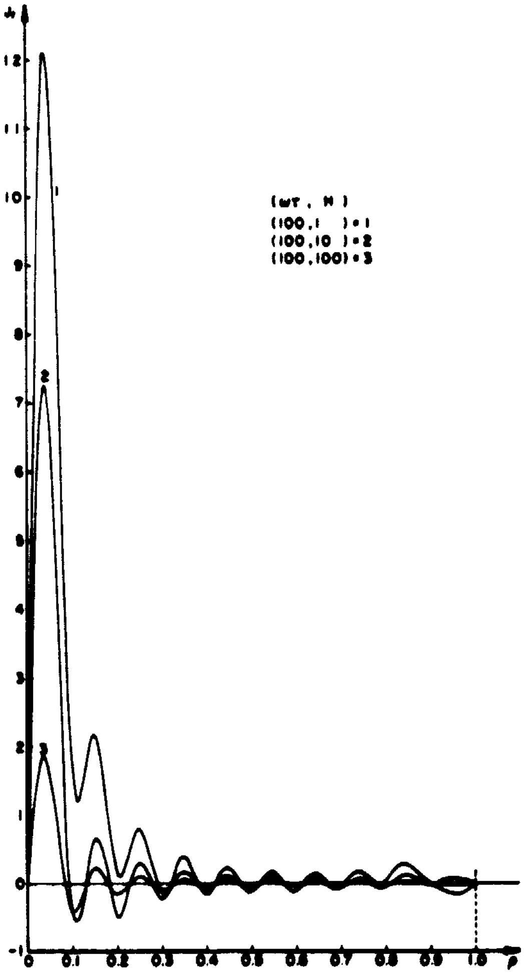

FIG. 30: J_r versus ρ for $\zeta = -0.9$, and $\omega\tau = 100$; $H = 1, 10, 100$.

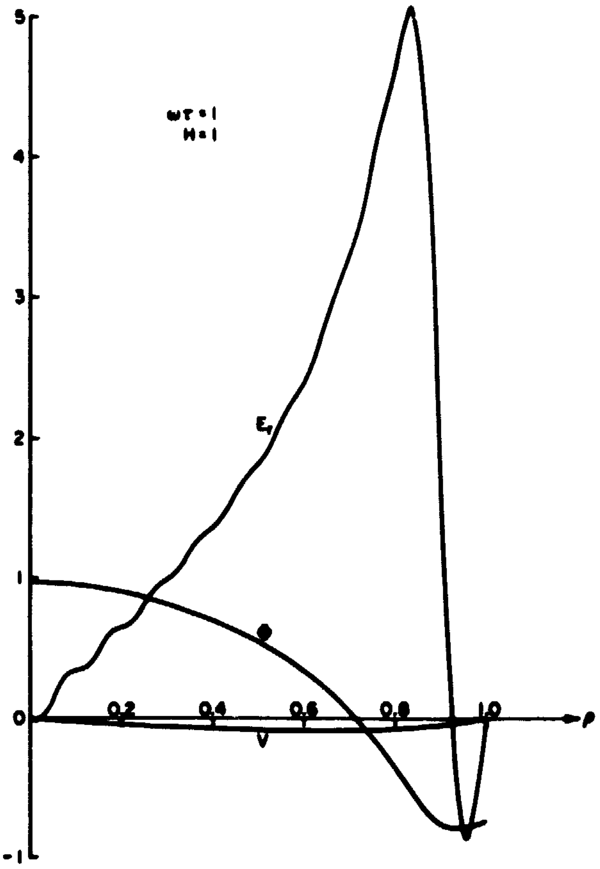

FIG. 31: Φ, E_r, and V versus ρ for ζ = +0.9, and ωτ = 1; H = 1.

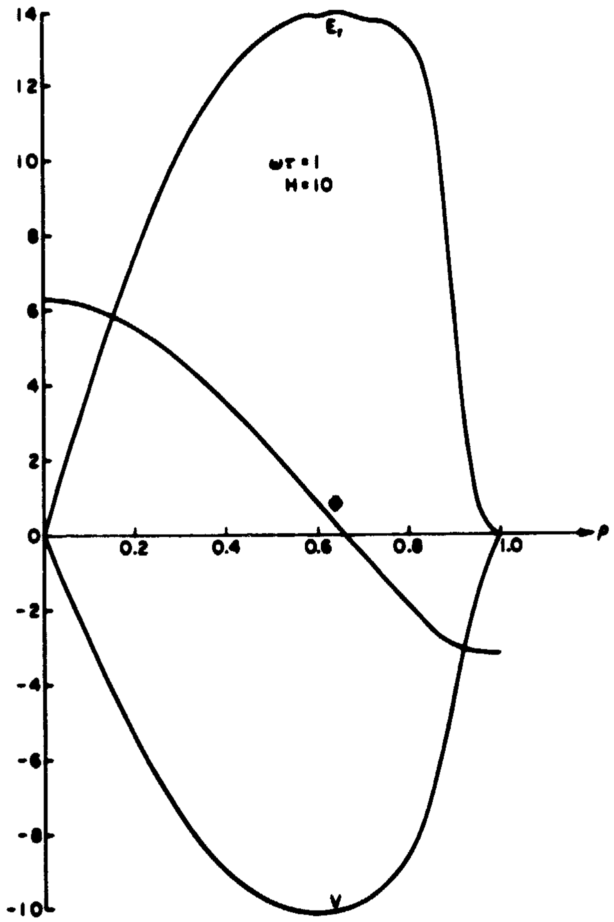

FIG. 32: Φ, E_r, and V versus ρ for $\zeta = +0.9$, and $\omega\tau = 1$; $H = 10$.

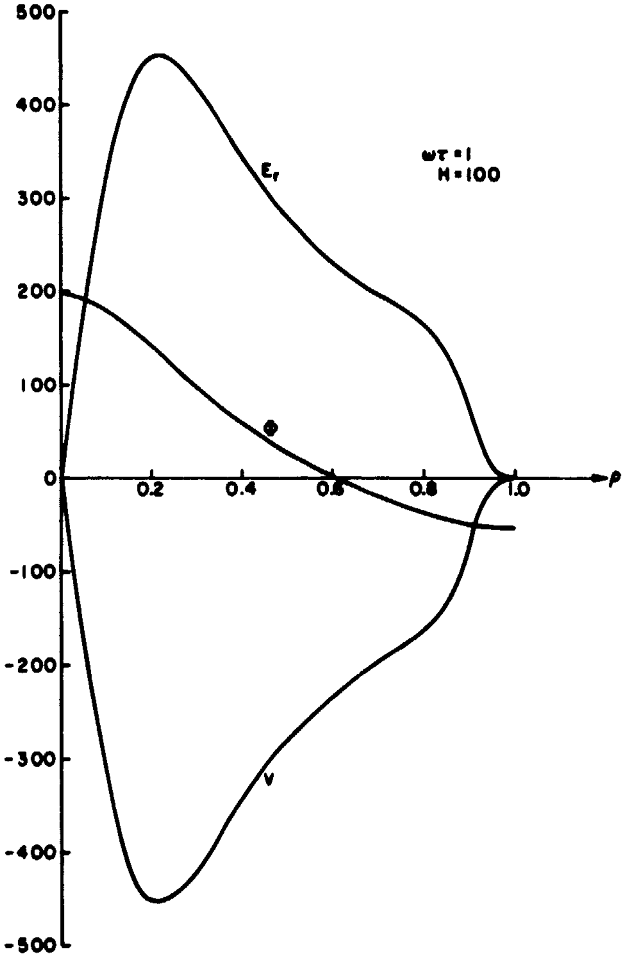

FIG. 33: Φ, E_r, and V versus ρ for $\zeta = +0.9$, and $\omega\tau = 1$; $H = 100$.

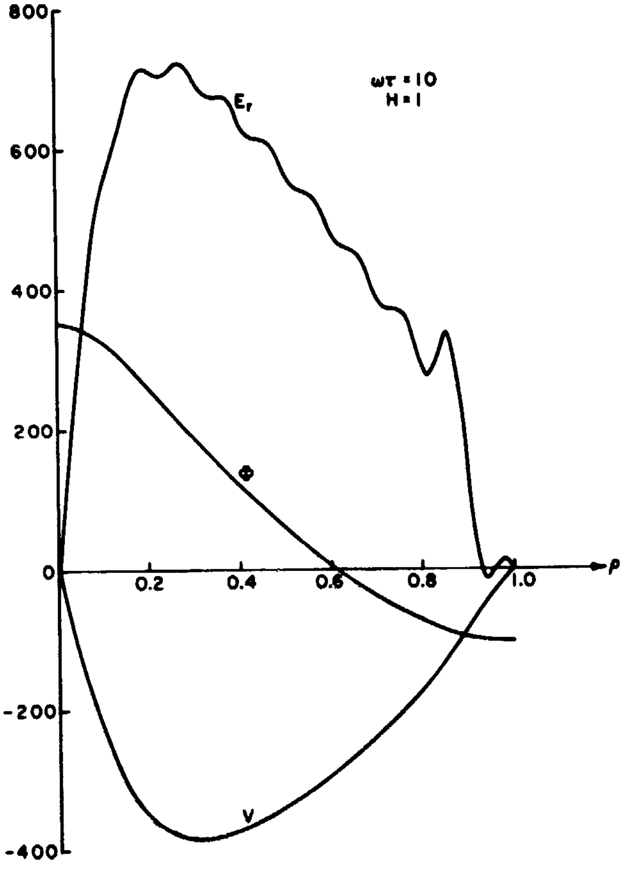

FIG. 34: Φ, E_r, and V versus ρ for $\zeta = +0.9$, and $\omega\tau = 10$; $H = 1$.

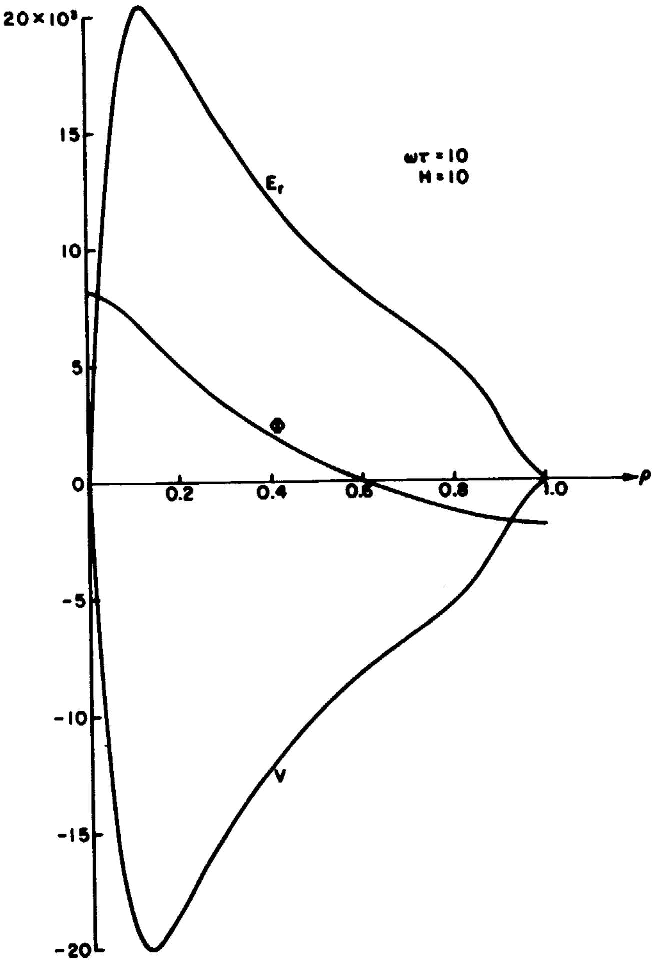

FIG. 35: Φ, E_r, and V versus ρ for $\zeta = +0.9$, and $\omega\tau = 10$; $H = 10$.

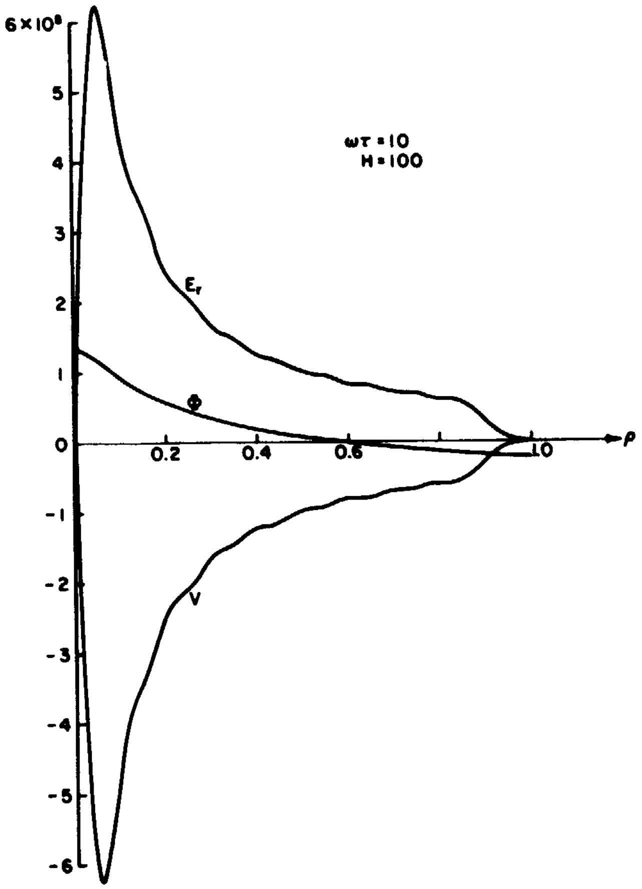

FIG. 36: Φ, E_r, and V versus ρ for $\zeta = +0.9$, and $\omega\tau = 10$; $H = 100$.

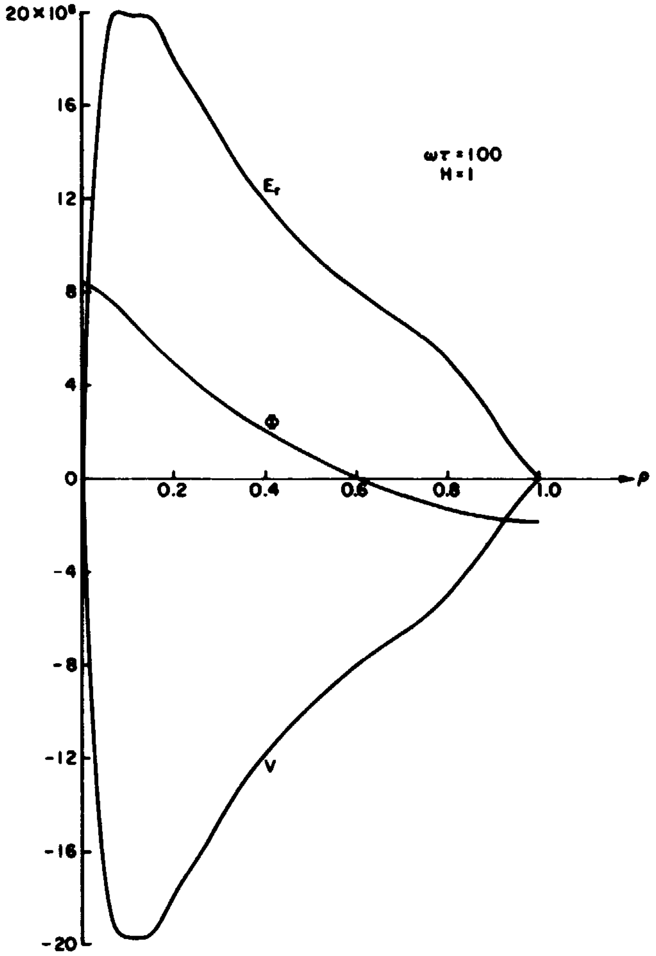

FIG. 37: Φ, E_r, and V versus ρ for ζ = +0.9, and ωτ = 100; H = 1.

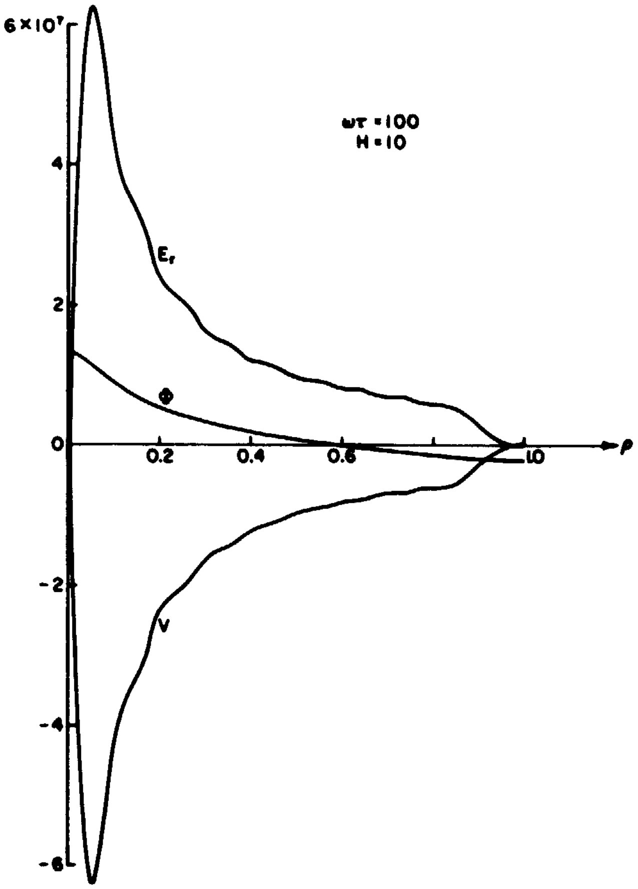

FIG. 38: Φ, E_r, and V versus ρ for $\zeta = +0.9$, and $\omega\tau = 100$; H = 10.

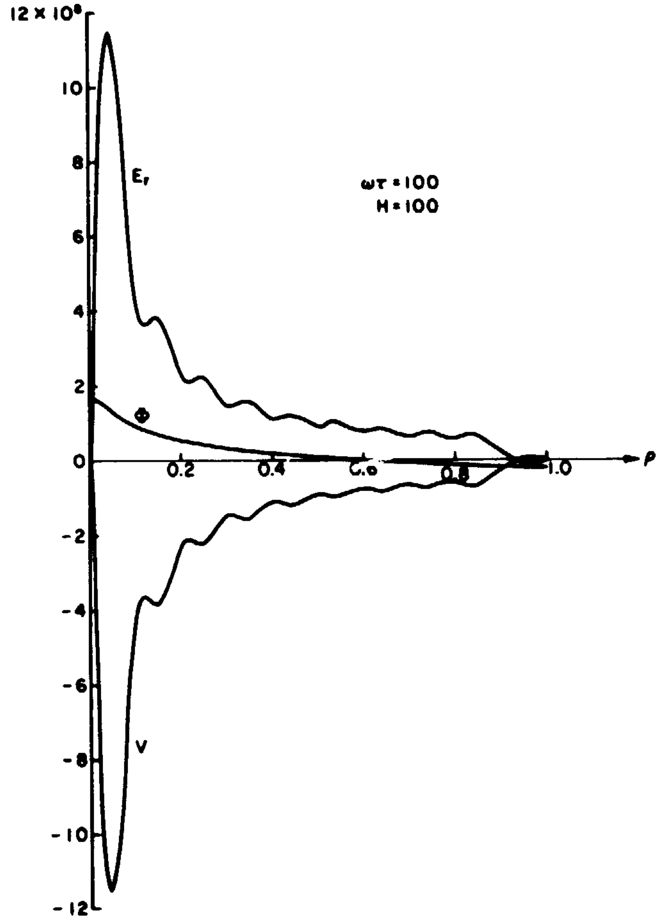

FIG. 39: Φ, E_r, and V versus ρ for $\zeta = +0.9$, and $\omega\tau = 100$; $H = 100$.

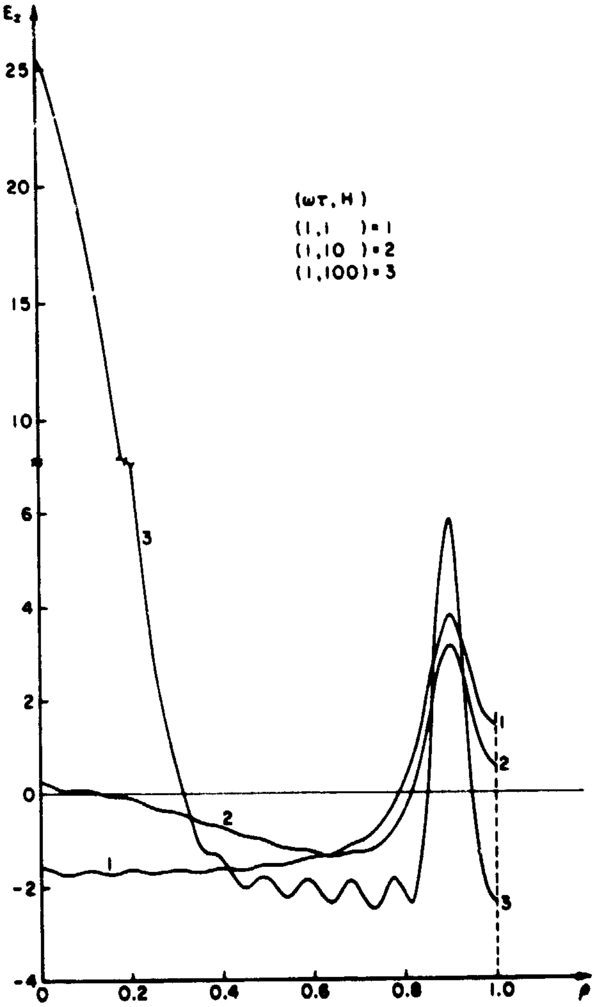

FIG. 40: E_z versus ρ for $\zeta = +0.9$, and $\omega\tau = 1$: $H = 1, 10, 100$.

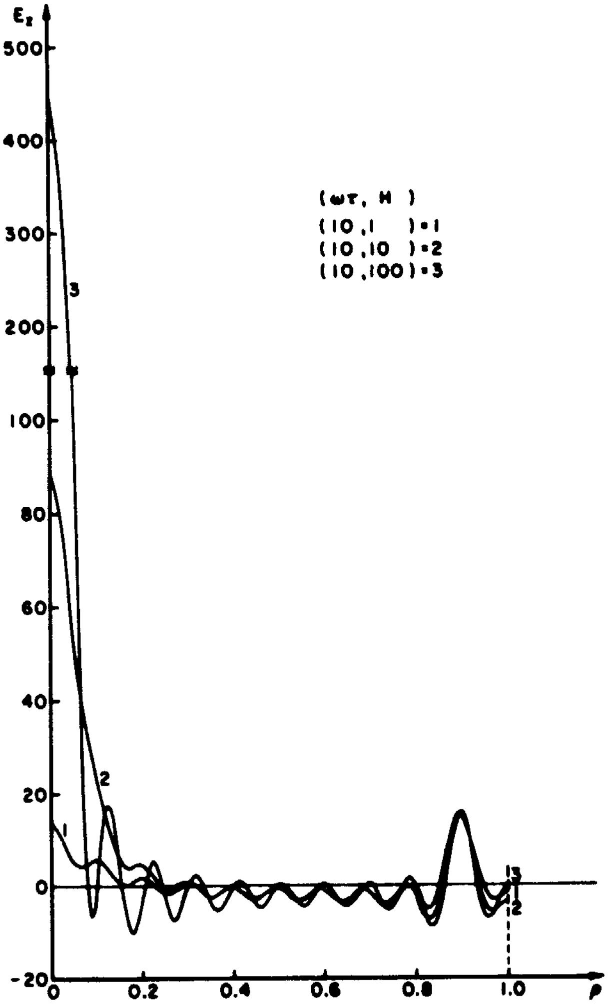

FIG. 41: E_z versus ρ for $\zeta = +0.9$, and $\omega\tau = 10$; $H = 1, 10, 100$.

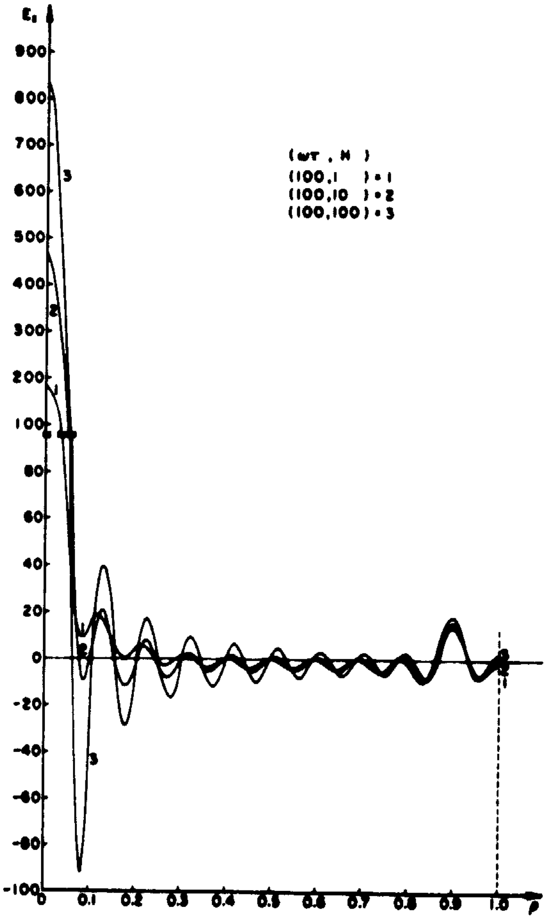

FIG. 42: E_z versus ρ for $\zeta = +0.9$, and $\omega\tau = 100$; $H = 1, 10, 100$.

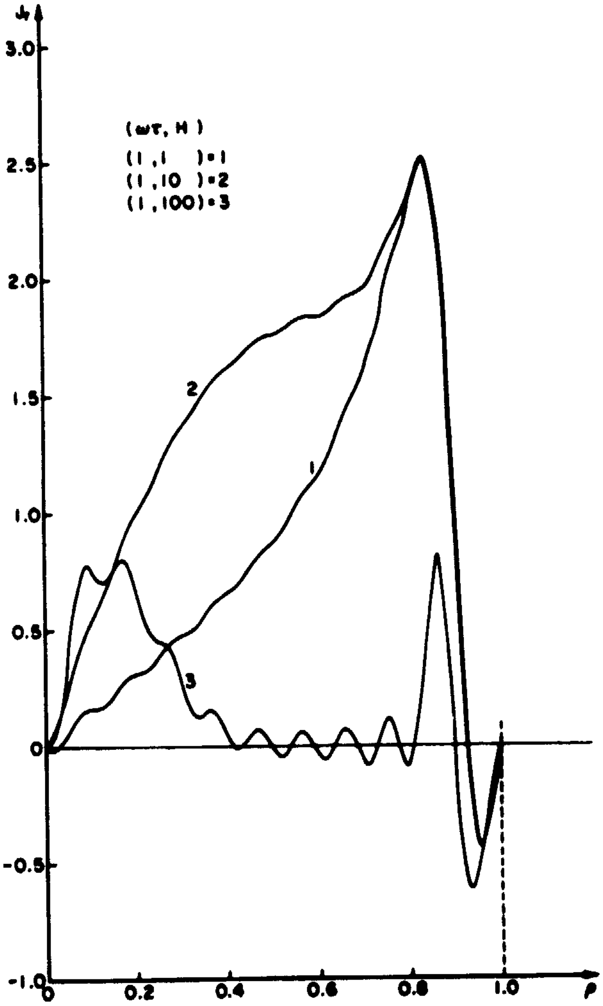

FIG. 43: J_r versus ρ for $\zeta = +0.9$, and $\omega\tau = 1$; H = 1, 10, 100.

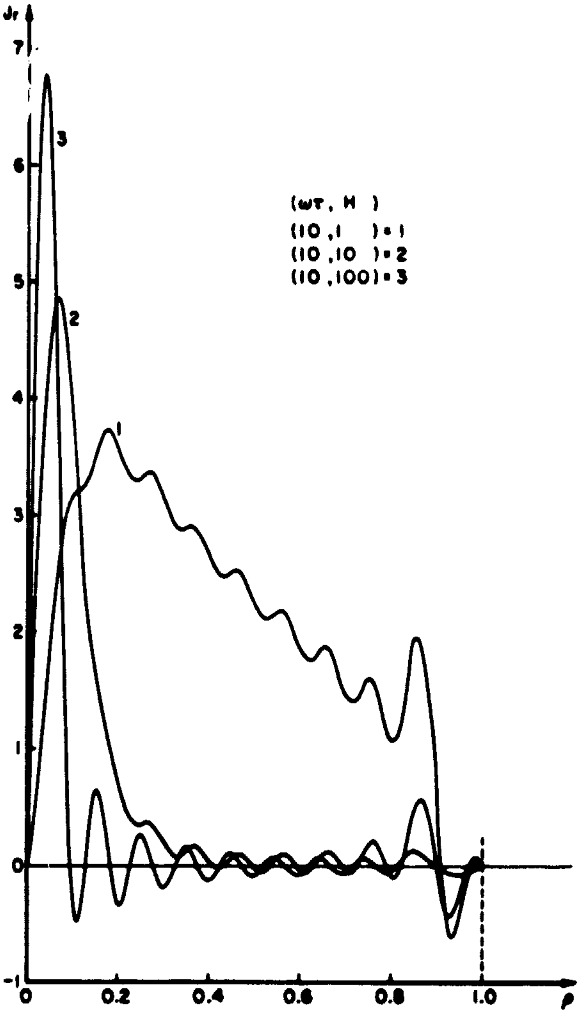

FIG. 44: J_r versus ρ for $\zeta = +0.9$, and $\omega\tau = 10$; $H = 1, 10, 100$.

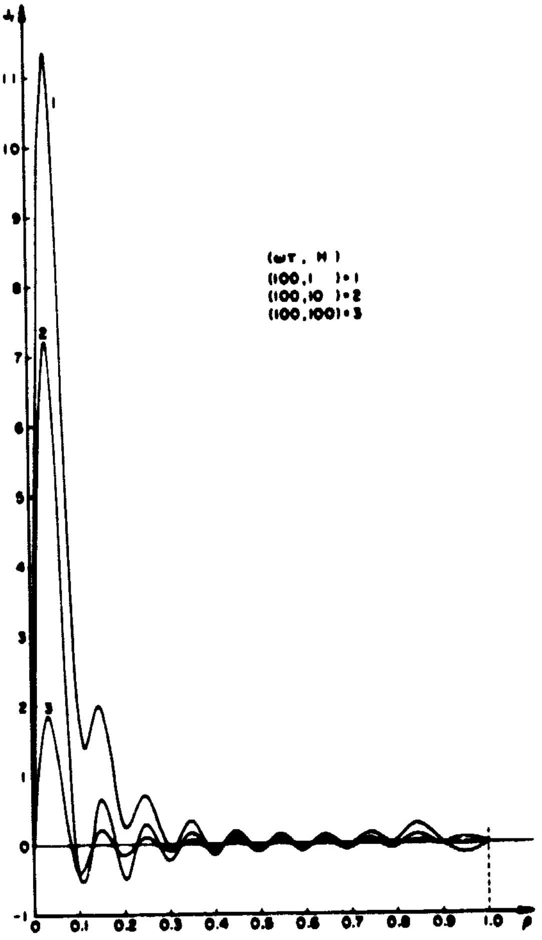

FIG. 45: J_r versus ρ for ζ = +0.9, and $\omega\tau$ = 100; H = 1, 10, 100.

QUANTUM THEORY OF SPUTTERING:

Application to Cross Section Determination

Abstract

Surface sputtering of polycrystalline metals is explained theoretically by means of a 3-body sputtering mechanism involving the impinging ion and two metal atoms. By means of quantum-mechanical perturbation theory, a formula for the number S(E) of atoms sputtered on the average by an ion of energy E is derived from first principles. The theory agrees with experimental sputtering data in the low energy region above the threshold. As an application mercury-metal atom scattering cross sections are determined by quantitative comparison of the theoretical and experimental S(E)-values for sputtering mercury ions and various metals.

By means of quantum-mechanical perturbation theory,[1)] the probability S(E) for an atom sputtered by an ion of energy E incident on a polycrystalline metal is calculated for low ion energies, $E \geq E_o$, where E_o is the apparent sputtering threshold. Whereas the previous classical approaches to the analysis of sputtering[2-10)] contain phenomenological parameters (usually determined by fitting the experimented S(E)-curves), the quantum-mechanical sputtering theory is based on first principles. The theory presented agrees with experimental sputtering data for low ion energies.[11,12)] As an application, the formula derived for the sputtering ratio S(E) is used for the determination of the total scattering cross section for mercury atoms (recombined Hg-ions) interacting with atoms of various metallic solids from the corresponding experimental sputtering data.[11,12)]

A binary collision between a surface atom of the solid and an ion incident normal to the surface can evidently not lead to sputtering since the atom does not acquire a momentum component in the direction of the external normal of the surface. Similarly, sputtering is not likely to occur for smaller angles of ion incidence if its energy is not large compared to the threshold energy for sputtering. It is evident that sputtering, at ion energies of the order of the threshold energy, is a 3-body process involving one ion and two surface atoms of the solid. At higher ion energies, however, sputtering will result mainly from higher order many-body interactions.

By restricting the theoretical considerations to ion energies E of the order of the threshold energy, $E \geq E_o$, sputtering is regarded as the result of an ion-atom-atom interaction. Furthermore, it is assumed that the solid is polycrystalline and has a sublimation energy which is on the average $E_s = < E_s^{ijk} >$, where the average is taken over the randomly distributed surfaces (ijk) of the crystallites. In this case, the sublimation energy E_s represents the average binding energy of a surface atom of the polycrystalline solid.

In the 3-body sputtering process, the incident ion transfers, on the average, the energy E_s (as well as kinetic energy) to the atom which is expelled and the energy α) $2E_s$ or β) $4E_s$ to the other atom depending on whether the latter is pushed to an α) unstable or β) stable interstitial lattice position. Accordingly, the threshold energies for the 3-body interactions α) and β) are:

$$E_\alpha = E_s + 2E_s = 3E_s \ ,$$

$$E_\beta = E_s + 4E_s = 5E_s \ .$$

Depending on whether the process α) or β) occurs with dominant probability, the apparent threshold (obtained by extrapolation of the experimental S(E)-curve, $E \to E_o$) will be $E_o \simeq E_\alpha$ or $E_o \simeq E_\beta$. If the cases α) and β) have equal probability one might introduce an average threshold by

$$\overline{E}_o = \frac{1}{2}(E_1 + E_2) = 4E_s \ .$$

Indeed, some of the experimentally found thresholds E_o(exper)$^{\underline{11},\underline{12})}$ can be explained by the theoretical formula $\overline{E}_o = 4E_s$. In other cases, the formulae $E_\alpha = 3E_s$ and $E_\beta = 5E_s$ have to be used to explain the measured thresholds. This is demonstrated in Table I which compares the experimental$^{\underline{11},\underline{12})}$ and theoretical threshold energies (E_α, E_β, $\overline{E}_o$) for different metals. Sputtering is in general not a simple threshold process which can be defined by means of a single threshold value. This will be shown in detail through the following quantum-statistical considerations.

TABLE I: Comparison of experimental and theoretical sputtering thresholds.

Target Element	Crystal Structure	E_o(theor) [eV]	E_o(exper) [eV]
Ag	fcc	$5E_S = 16.75$	17
Au	fcc	$3E_S = 11.70$	18
Co	hcp	$5E_S = 22.00$	22
Cu	fcc	$5E_S = 17.65$	17
Fe	bcc	$5E_S = 20.60$	20
Mo	bcc	$4E_S = 24.80$	24
Nb	bcc	$4E_S = 30.84$	32
Pt	fcc	$3E_S = 16.80$	22
Ta	bcc	$3E_S = 24.00$	25
Ti	hcp	$5E_S = 24.20$	25
W	bcc	$4E_S = 35.20$	35
Zr	hcp	$3E_S = 18.42$	18

In Table I, the experimental thresholds have been taken from Stuart and Wehner[11]. These authors concluded from their experimental data that the threshold is independent from the mass ratio between the incident ion and target atom,[11] and is, in first approximation, equal to $\bar{E}_o = 4E_S$, the average displacement threshold in radiation damage.[11] It is seen that the agreement between the theoretical thresholds ($E_{\alpha,\beta}$, $\bar{E}_o$) and the experimental values E_o(exper) is excellent, except in the cases Au and W. Whether the α-process or the β-process is dominant or both are (about) equally probable is apparently not dependent on the respective crystal system (fcc, bcc, hcp).

PERTURBATION THEORY

In general, a sputtering ion recombines with an electron into an atom as soon as it approaches the surface of a metal.[9)] This means that the incident ion interacts actually like a neutral atom with the atoms of the solid. This neutralized ion is always referred to as "ion", in order to distinguish it from the "atoms" of the solid. Experiments indicate that also the atom sputtered from the metal surface is electrically neutral.[9)]

When an ion of low energy as defined above hits the surface of a solid, one of the following processes may occur: 1) the ion is reflected without energy loss by the bound surface atom it encounters; 2) the ion collides with a surface atom and quasi-simultaneously with a second atom so that 3-body sputtering results. The total probability for the ion to interact in either of the two ways with the solid is

$$P_N = N^{2/3}\sigma(E) \tag{1}$$

where N is the number density of atoms in the solid and $\sigma(E)$ is the total (energy dependent) cross section for ion-atom scattering. Let $w_1(E)$ and $w_2(E)$ be the transition probability rates for the processes 1) and 2), respectively. The relative probability with which sputtering occurs is then

$$W_s(E) = \frac{w_2(E)}{w_1(E) + w_2(E)} \approx \frac{w_2(E)}{w_1(E)}\,, \quad w_2(E) << w_1(E). \tag{2}$$

Combining of Eqs. (1) and (2) yields for the sputtering rate, i.e., the number of atoms expelled on the average by one ion of energy E from the solid,

$$S(E) = \sigma(E)N^{2/3}\,W_s(E) \quad . \tag{3}$$

On principle, $\sigma(E)$ can be calculated quantum mechanically, or determined experimentally.

In the transition processes 1) or 2), the ion interacts with the surface of the solid within an area of the extension of the de Broglie wavelength, $\lambda = \hbar/\sqrt{2mE}$. For this reason, the spatial part of the phase space is

$$V = \frac{4\pi}{3}R^3,\ R \approx \hbar/(2mE)^{1/2} \quad . \tag{4}$$

The transition probability $w(E)$ from a state "i" to a state "f" is proportional to the matrix element $|M_{if}|$ in square and the density of final states $d\rho/dE$ per unit energy,[1)]

$$w(E) = \frac{2\pi}{\hbar}|M_{if}|^2\frac{d\rho}{dE} \quad , \tag{5}$$

where

$$M_{if} = \iiint_{\Omega} \psi_f^{*}\tilde{H}\,\psi_i\, d^3\vec{r} \quad , \tag{6}$$

and

$$\frac{d\rho}{dE} = \left[\frac{\Omega}{(2\pi\hbar)^3}\right]^n \frac{d\Phi(E)}{dE} \tag{7}$$

for a state containing n independent particles with moments $\vec{p}_1, \vec{p}_2, \ldots, \vec{p}_n$. $\Phi(E)$ is the volume of momentum space corresponding to the total energy E. $\tilde{H}$ is the perturbation (operator) of the Hamiltonian of the ion-atom system which causes the transition $i \rightarrow f$, and ψ_i and ψ_f are the wave functions of the total system before and after the transition which are normalized for the volume Ω, $\Omega > V$.

Equations (5) through (7) represent the basis for the determination of the process probabilities $w_1(E)$ and $w_2(E)$.

1. Reflection State. $w_1(E)$ is defined as the probability rate for the ion to be reflected at the surface of the solid without energy loss. In the center of mass system, the ion momentum is $p = \sqrt{2mE}$ in the final state and the momentum space volume is $\Phi(E) = 4\pi p^3/3$. According to Eqs. (5) through (7), the transition probability for reflection is per unit time $(n=1)$

$$w_1(E) = \frac{2\pi}{\hbar} |M_{if}^{(1)}|^2 \, [\Omega/(2\pi\hbar)^3] \, 2\pi\sqrt{2}m^{3/2} \, E^{1/2} \qquad (8)$$

where $M_{if}^{(1)}$ is the matrix element of the transition 1).

2. Sputtering State. $w_2^{\sigma}(E)$ is defined as the probability rate for the 3-body sputtering state with threshold E_σ, $\sigma = \alpha, \beta$ $(E_\alpha = 3E_s,\ E_\beta = 5E_s)$. In the center of mass system, the momenta of the ion (i), the sputtered atom (s), and the second atom (a) can be chosen as

$$\vec{p}_i = \vec{p},\ \vec{p}_s = -\frac{1}{2}\vec{p} - \vec{q},\ \ \vec{p}_a = -\frac{1}{2}\vec{p} + \vec{q} \quad , \qquad (9)$$

so that momentum is conserved $\Sigma_j \vec{p}_j = \vec{0}$. Since the potential energy E_σ is expended in the sputtering interaction of type $\sigma = \alpha,\ \beta$, the total kinetic energy of the three particles is

$$E^* = E - E_\sigma = \left(\frac{1}{2m} + \frac{1}{4M}\right)\vec{p}^{\,2} + \frac{1}{M}\vec{q}^{\,2} \geq 0 \quad . \qquad (10)$$

Equation (10) represents an ellipsoid with the axes sections $\{4[mM/(m + 2M)]E^*\}^{1/2}$ and $(ME^*)^{1/2}$ in the six-dimensional space of the vectors $\vec{p}$ and $\vec{q}$. Hence, the volume of the momentum space is

$$\Phi(E) = \frac{\pi^3}{6}\left(\frac{4mM^2}{m + 2M}\right)^{3/2} (E - E_\sigma)^3 \geq 0 \qquad . \qquad (11)$$

From Eqs. (5) through (7) and (11) one obtains the transition probability for the sputtering state with threshold E_σ per unit time (n=2)

$$w_2^\sigma(E) = \frac{2\pi}{\hbar} [\Omega/(2\pi\hbar)^3]^2 \, |M_{if}^{(2)}|^2 4\pi^3 \left(\frac{mM^2}{m + 2M}\right)^{3/2} (E - E_\sigma)^2 \, H(E - E_\sigma) \qquad (12)$$

where $M_{if}^{(2)}$ is the matrix element of the transition 2) and $H(E - E_\sigma) = 1$ or 0 for $E \geq E_\sigma + 0$ or $E \leq E_\sigma - 0$ (Heaviside).

With the assumption $w_2^\sigma(E) << w_1(E)$, one obtains from Eqs. (2), (8), and (12) for the relative sputtering probability the expression,

$$W_s^\sigma(E) = \frac{\Omega}{8\pi\sqrt{2}} \, \frac{|M_{if}^{(2)}|^2}{|M_{if}^{(1)}|^2} \left(\frac{M^2}{m + 2M}\right)^{3/2} \frac{(E - E_\sigma)^2}{E^{1/2}} \, H(E - E_\sigma) \ . \qquad (13)$$

The matrix elements $|M_{if}^{(1,2)}|$ in square are proportional to the probabilities for finding the interacting particles in the processes 1) and 2) in the interaction volume V [Eq. (1)], i.e.,

$$|M_{if}^{(1)}|^2 \propto (V/\Omega)^1, \quad |M_{if}^{(2)}|^2 \propto (V/\Omega)^2 \qquad , \qquad (14)$$

since these are one and two independent particles in the interactions 1) and 2), respectively. Substitution of Eqs. (14) and (4) into Eq. (13) leads to the following equation for the relative probability for sputtering with threshold E_σ ($\sigma = \alpha, \beta$):

$$W_s^\sigma(E) \doteq \frac{h_{2/1}}{24} \left[\frac{(M/m)^2}{1 + 2(M/m)}\right]^{3/2} \frac{(E - E_\sigma)^2}{E^2} \, H(E - E_\sigma) \qquad . \qquad (15)$$

$h_{2/1} \equiv (\Omega/V) \, |M_{if}^{(2)}|^2/|M_{if}^{(1)}|^2$ is a correction factor of the magnitude $O[h_{2/1}] = 1$, which can be determined more accurately by evaluating the matrix elements if the force potentials of the interactions 1) and 2) are known.

SPUTTERING RATIO

In the sputtering of a surface atom by an ion, two fundamental cases (α) and (β) are distinguished which have the thresholds $E_\alpha = 3E_s$ and $E_\beta = 5E_s$, respectively. Let the probabilities for the occurrence of the thresholds E_α and E_β be g_α and g_β, which are normalized in the usual way,

$$g_\alpha + g_\beta = 1, \quad g_{\alpha,\beta} > 0 \quad . \tag{16}$$

It follows for the relative probability that sputtering occurs with either of the thresholds E_α and E_β,

$$W_s = \sum_{\sigma=\alpha,\beta} g_\sigma W_s^\sigma \tag{17}$$

Substitution of Eqs. (17) and (15) into Eq. (3) yields for the number of atoms sputtered on the average by an ion of energy E:

$$S(E) = \frac{h_{2/1}}{24} \sigma(E) N^{2/3} \left[\frac{(M/m)^2}{1 + 2(M/m)}\right]^{3/2} \sum_{\sigma=\alpha,\beta} g_\sigma \frac{(E - E_\sigma)^2}{E^2} H(E - E_\sigma) . \tag{18}$$

For applications, it is suitable to further simplify Eq. (18), which is strictly valid only for ion energies $E \geq E_{\alpha,\beta}$. For example, if only one threshold $E_0 \; \varepsilon (E_\alpha, E_\beta)$ is important ($g_\alpha << 1$ or $g_\beta << 1$) and the total scattering cross section $\sigma(E)$ varies slowly at $E \simeq E_0$ (absence of resonances), Eq. (18) can be reduced to

$$S(E) = \frac{h_{2/1}}{24} \sigma(E_0) N^{2/3} \left[\frac{(M/m)^2}{1 + 2(M/m)}\right]^{3/2} \frac{(E - E_0)^2}{{E_0}^2} H(E - E_0) \tag{19}$$

with

$$\sigma(E)/E^2 = \sigma(E_0)/{E_0}^2, \quad E \geq E_0 \; . \tag{20}$$

Equation (19) is exactly of the form of the sputtering relation $S(E) = \text{const}(E - E_o)^2$ found phenomonologically by fitting experimental sputtering data.[11) It is commonly used in the extrapolation $E \to E_o$ of experimental data to find the threshold E_o.[11) Recently, also a relation $S(E) = \text{const}(E - E_o)^3$ has been employed in the extrapolatory determination of the threshold E_o,[12) which appears to be difficult to justify theoretically. As expected, the thresholds reported in Refs. 11 and 12 are in general somewhat different.

APPLICATION

In the literature, measurements of the total scattering cross sections for Hg-atoms (recombined ion) and target atoms such as Ag, Au, Co, Cu, Fe, Mo, Nb, Pt, Ta, Ti, W, Zr have apparently not been reported.13) Theoretical cross section values are not available yet owing to the mathematical difficulties associated with the application of quantum mechanical scattering theory to many-electron atoms.14) For these reasons, the cross sections under consideration shall be determined here by comparing the theoretical [Eq. (19)] and experimental sputtering ratios $S(E)$.

In Figs. 1-12, the dashed curves represent the experimental sputtering data of Askerov and Sena12) for Hg ions and the (polycristalline) target materials Ag, Au, Co, Cu, Fe, Mo, Nb, Pt, Ta, Ti, W and Zr (with the lowest $S(E)$ value measured at $E = \hat{E}$ indicated by a dot). The corresponding theoretical sputtering curves $S(E)$, based on Eq. (19) and the theoretical thresholds given in Table I, are shown by solid lines. The cross section values $\sigma(E_o)$ are chosen in such a way that the experimental and theoretical sputtering curves agree in the low energy region $E \gtrsim \hat{E}$, since theory and experiment should agree the better the lower the ion energy is (3-body sputtering model). The mass of Hg is $m = 200.59$ a.m.u., and the remaining constants M and N in Eq. (19) are given in Table I. The latter shows also the details of the calculation of the cross sections $\sigma(E_o)$ from the experimental sputtering data by means of Eq. (19). It is seen that the cross sections $\sigma(E_o)$ for atom-atom scatterings are between 10^0 to 10^1 barns at low energies, i.e. are of the order-of-magnitude expected ($h_{2/1} \doteq 1$).

TABLE II

Constants of Sputtering Formula and Cross Sections $\sigma(E_o)$ for Various Target Atoms

Target Atoms	M[gr]	$[\frac{(M/m)^2}{1+2M/m}]^{3/2}$	$N[cm^{-3}]$	$N^{2/3}[cm^{-2}]$	$[h_{2/1}\sigma(E_o)N^{2/3}/24]_{exper}$	$h_{2/1}\sigma(E_o)[cm^2]$
Ag	1.7906×10^{-22}	5.201×10^{-2}	5.859×10^{22}	1.509×10^{15}	8.700×10^{-2}	1.384×10^{-15}
Au	3.2697×10^{-22}	1.856×10^{-1}	5.903×10^{22}	1.516×10^{15}	2.672×10^{-2}	4.230×10^{-16}
Co	9.7829×10^{-23}	1.268×10^{-2}	8.903×10^{22}	1.994×10^{15}	9.687×10^{-2}	1.166×10^{-15}
Cu	1.0549×10^{-22}	1.523×10^{-2}	8.468×10^{22}	1.928×10^{15}	1.993×10^{-1}	2.480×10^{-15}
Fe	9.2706×10^{-23}	1.111×10^{-2}	8.478×10^{22}	1.930×10^{15}	7.649×10^{-2}	9.512×10^{-16}
Mo	1.5926×10^{-22}	3.998×10^{-2}	5.657×10^{22}	1.474×10^{15}	2.248×10^{-2}	3.661×10^{-16}
Nb	1.5422×10^{-22}	3.716×10^{-2}	5.187×10^{22}	1.391×10^{15}	3.719×10^{-2}	6.417×10^{-16}
Pt	3.2385×10^{-22}	1.820×10^{-1}	6.599×10^{22}	1.633×10^{15}	2.244×10^{-2}	3.298×10^{-16}
Ta	3.0037×10^{-22}	1.563×10^{-1}	5.526×10^{22}	1.451×10^{15}	9.593×10^{-3}	1.587×10^{-16}
Ti	7.9514×10^{-23}	7.581×10^{-3}	5.659×10^{22}	1.474×10^{15}	1.786×10^{-1}	2.908×10^{-15}
W	3.0519×10^{-22}	1.615×10^{-1}	6.324×10^{22}	1.587×10^{15}	1.344×10^{-2}	2.032×10^{-16}
Zr	1.5143×10^{-22}	3.564×10^{-2}	4.253×10^{22}	1.218×10^{15}	2.658×10^{-2}	5.236×10^{-16}

The Figs. 1-12 indicate that the theoretical sputterings formula in Eq. (19) describes the experimental data rather well in the low energy region $E \gtrsim E_o$. The theoretical sputtering curves $S(E)$ are plotted up to $E = 120$ eV, in order to show the deviations of Eq. (19) from the experimental data at larger ion energies, E. The 3-body sputtering model and the sputtering formula derived from it evidently represent adequate approximations only up to energies $E = 2E_o$ to $3E_o$.

It should be noted that the theoretical sputtering curves [Eq. (19)] are very sensitive towards changes in the thresholds E_o. It can be shown that an adequate agreement between the experimental and theoretical sputtering curves $S(E)$ cannot be obtained by choosing theoretical thresholds E_o noticeably different from those in Table I and varying the values of the cross sections $\sigma(E_o)$. Experimental or theoretical cross section values are obviously necessary to demonstrate the success of the quantum mechanical sputtering theory presented in a rigorous way.

REFERENCES

1. L.I. Schiff, Quantum Mechanics, McGraw-Hill, New York (1955).
2. A. von Hippel, Ann. Physik. 80, 672 (1926).
3. F. Keywell, Phys, Rev. 97, 1611 (1955).
4. G.K. Wehner, Adv. Electron. Electr. Phys. VII, 239 (1956). Phys. Rev. 93, 633 (1954); 102, 690 (1956); 108, 35 (1957).
5. E.B. Henschke, Phys. Rev. 106, 737 (1957).
6. E. Langberg, Phys. Rev. III, 91 (1958).
7. D.E. Harrison, Phys. Rev. 102, 1473 (1956); 105, 1202 (1957); 122, 1421 (1961).
8. R.I. Garber and A.I. Federenko, UFN 83, 385 (1964).
9. M. Kaminsky, Atomic and Ionic Impact Phenomena on Metal Surfaces, Academic Press, New York (1965).
10. R. Behrisch, Ergebn. Exact. Nature. XXXV, 295 (1964).
11. R.V. Stuart and G.K. Wehner, J. Appl. Phys. 33, 2345 (1962).
12. S.G. Askerov and L.A. Sena, Sov. Phys.--Solid State 11, 1288 (1969).
13. H.S.W. Massey, E.H. Bruhop, and H.B. Gilbody, Electronic and Ionic Impact Phenomena, Clarendon Press, Oxford (1969).
14. N.E. Mott and H.S.W. Massey, The Theory of Atomic Collisions, Clarendon Press, Oxford (1965).

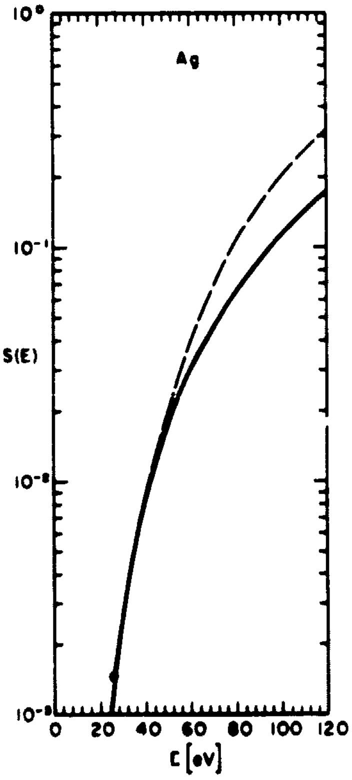

Fig. 1: Theoretical (——) and experimental (---) sputtering ratios S(E) for Ag.

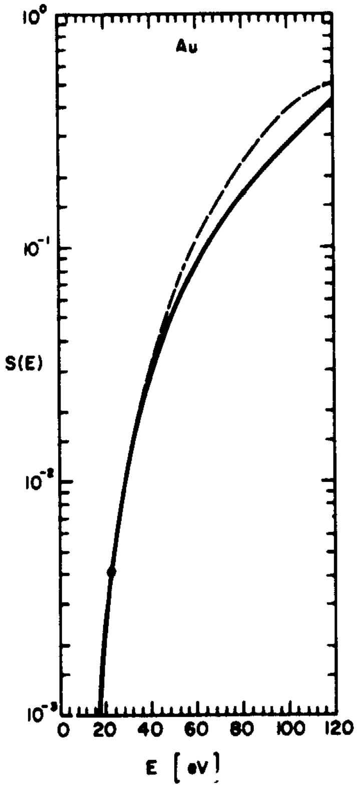

Fig. 2: Theoretical (——) and experimental (---) sputtering ratios S(E) for Au.

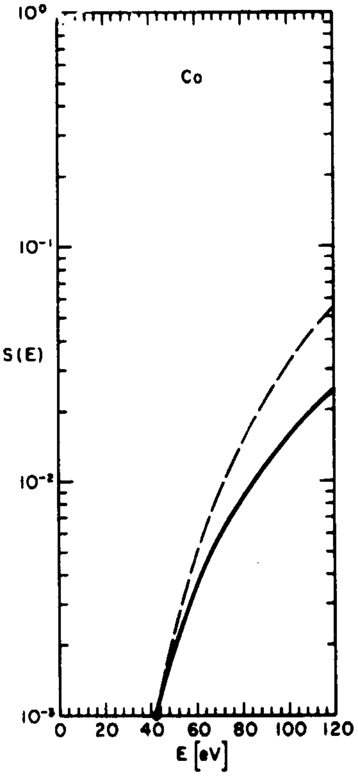

Fig. 3: Theoretical (——) and experimental (---) sputtering ratios S(E) for Co.

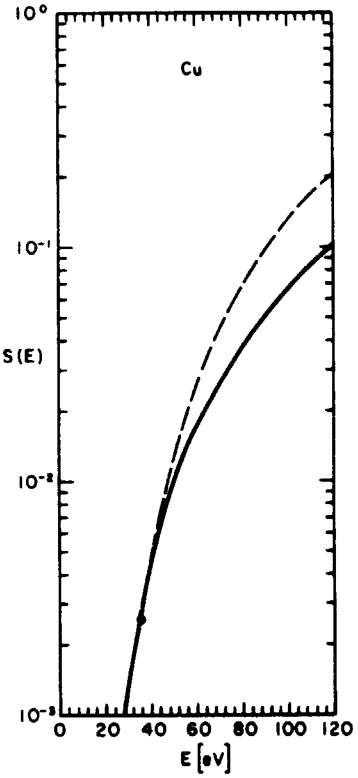

Fig. 4: Theoretical (——) and experimental (---) sputtering ratios S(E) for Cu.

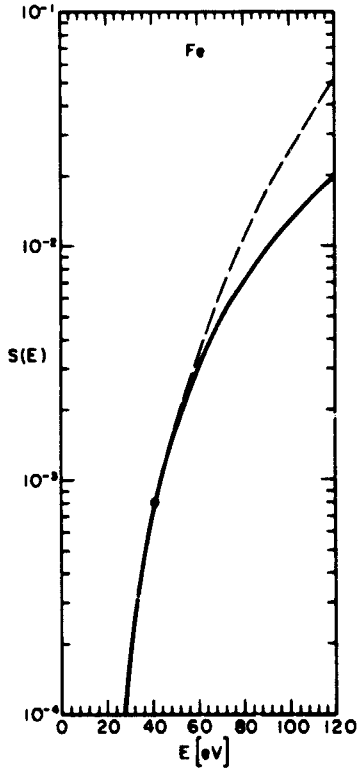

Fig. 5: Theoretical (——) and experimental (---) sputtering ratios S(E) for Fe.

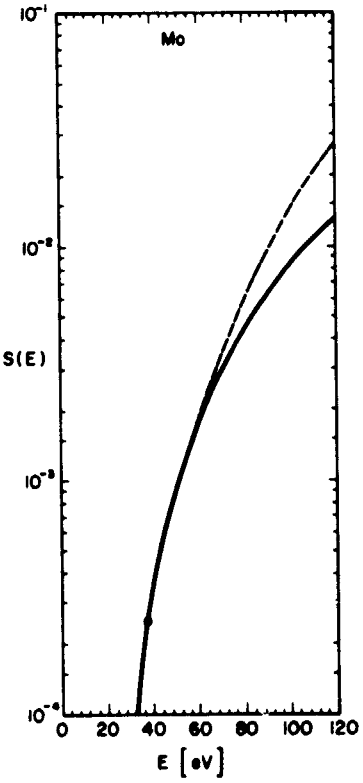

Fig. 6: Theoretical (——) and experimental (---) sputtering ratios S(E) for Mo.

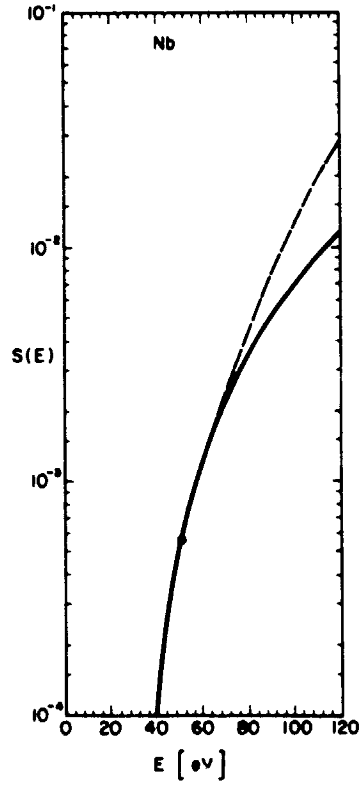

Fig. 7: Theoretical (——) and experimental (---) sputtering ratios S(E) for Nb.

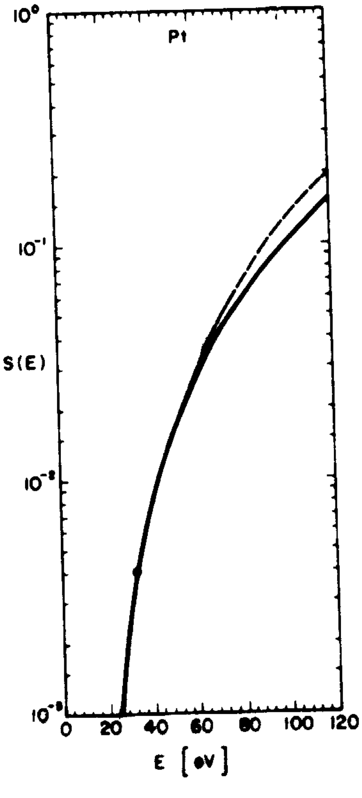

Fig. 8: Theoretical (——) and experimental (---) sputtering ratios S(E) for Pt.

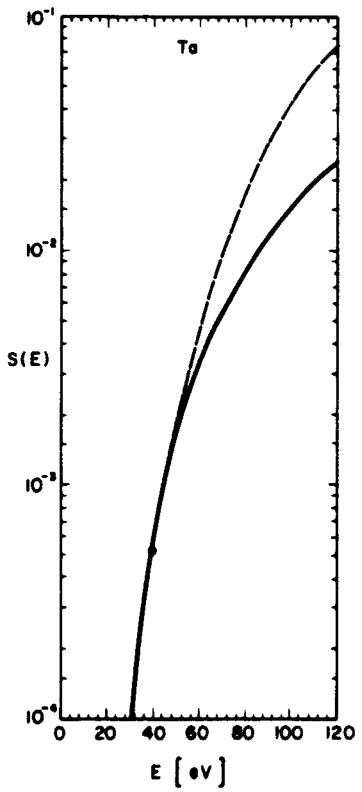

Fig. 9: Theoretical (——) and experimental (---) sputtering ratios S(E) for Ta.

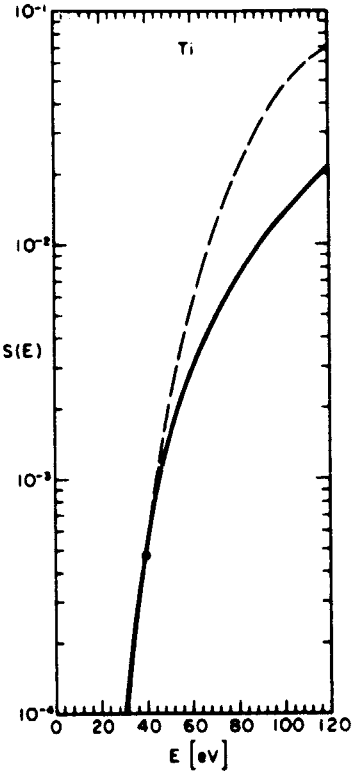

Fig. 10: Theoretical (——) and experimental (---) sputtering ratios S(E) for Ti.

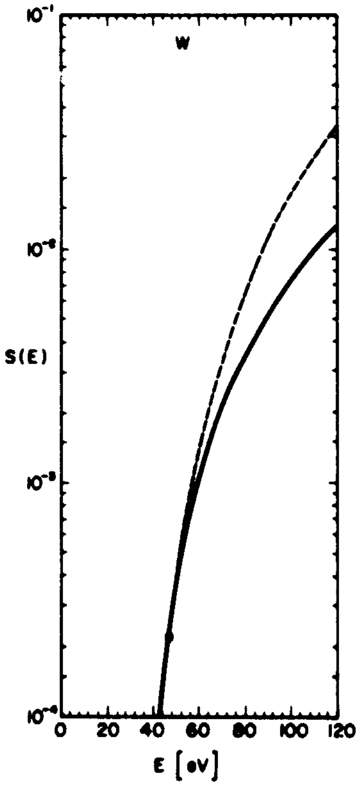

Fig. 11: Theoretical (——) and experimental (---) sputtering ratios S(E) for W.

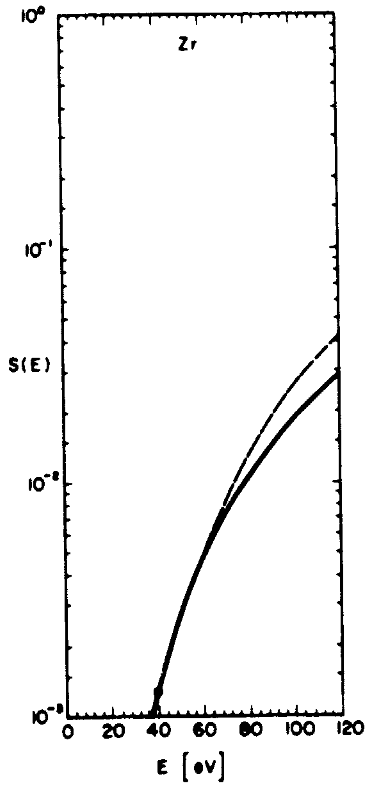

Fig. 12: Theoretical (——) and experimental (---) sputtering ratios S(E) for Zr.

DEPOSITION OF SPUTTERING PRODUCTS ON SYSTEM SURFACES

ABSTRACT

An analytical theory is developed describing the deposition of sputtered atoms on system surfaces which cannot be seen along straight paths from the emitting surface. The boundary-value problem describing the diffusion of the sputtered atoms through the surrounding rarefied electron-ion plasma to the "hidden" system surfaces is formulated and treated analytically. It is shown that outer boundary-value problems of this type lead to a complex integral equation, which requires numerical resolution.

In an ideal vacuum, sputtered atoms travel undeflected along straight paths determined by their initial velocities at the point of emission. Within this free particle flow, a system surface is reached by the sputtered atoms only if it can be seen along a straight line from the emitting surface. In reality, ion propulsion systems are surrounded by a very rarefied plasma consisting of escaped beam ions, recombined ions, and electrons. For this reason, always some of the sputtered atoms will be deflected out of their initial paths by interacting through long-range forces (polarization forces) with the plasma particles so that they can reach system surfaces which are not seen along a straight line from the emitter.

Figure 1 depicts the geometry of an idealized propulsion system which exhibits an emitting plane $z = 0$, $0 \leq r \leq a$ (accelerating grid), the rocket surfaces $r = a$, $-c \leq z \leq 0$ and $z = -c$, $0 \leq r \leq a$, and the plane $z = -d$, $a \leq r \leq b$ of the solar energy collectors. All these system surfaces can be reached by the atoms sputtered from the emitter by diffusion through the rarefied plasma. The diffusion coefficient D is determined by the Vlasov equation[1)] for the sputtered atoms interacting through weak long-range forces[1)] with the plasma particles. In view of the mathematical difficulties associated with the solution of outer boundary-value problems for the geometry in Fig. 1, a somewhat simpler system is studied here consisting of an emitting plane ($z = 0$, $0 \leq r \leq a$), the upper rocket surface ($r = a$, $-c \leq z \leq 0$) and the plane ($z = -c$, $a \leq r \leq \infty$) of the solar energy collectors (Fig. 2). The latter is assumed to have infinite radial extension, $r_{max} = b \to \infty$

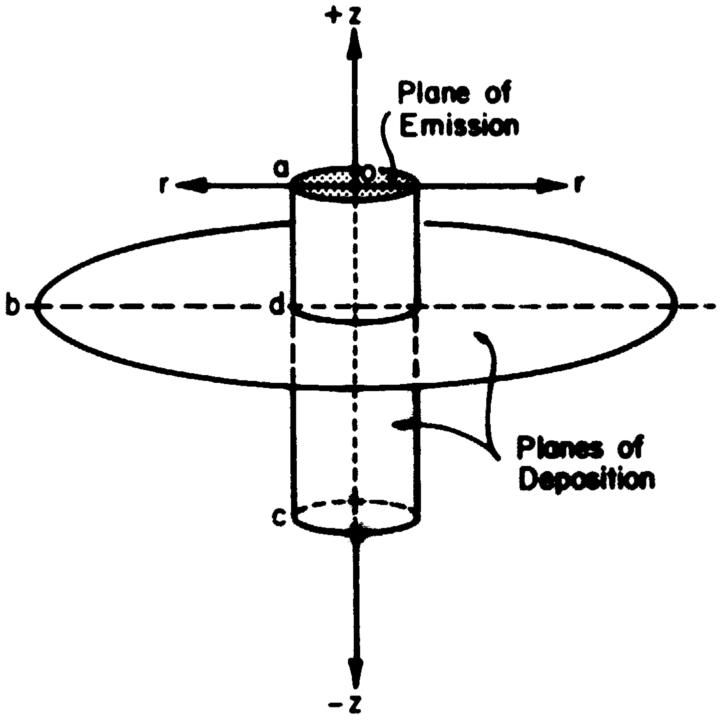

FIG.: 1

since in general b>>a and b>>c,d (Fig. 1). Within the model of Fig. 2, particle deposition on system surfaces in the space $z \leq -c$ cannot be analyzed.

C-2

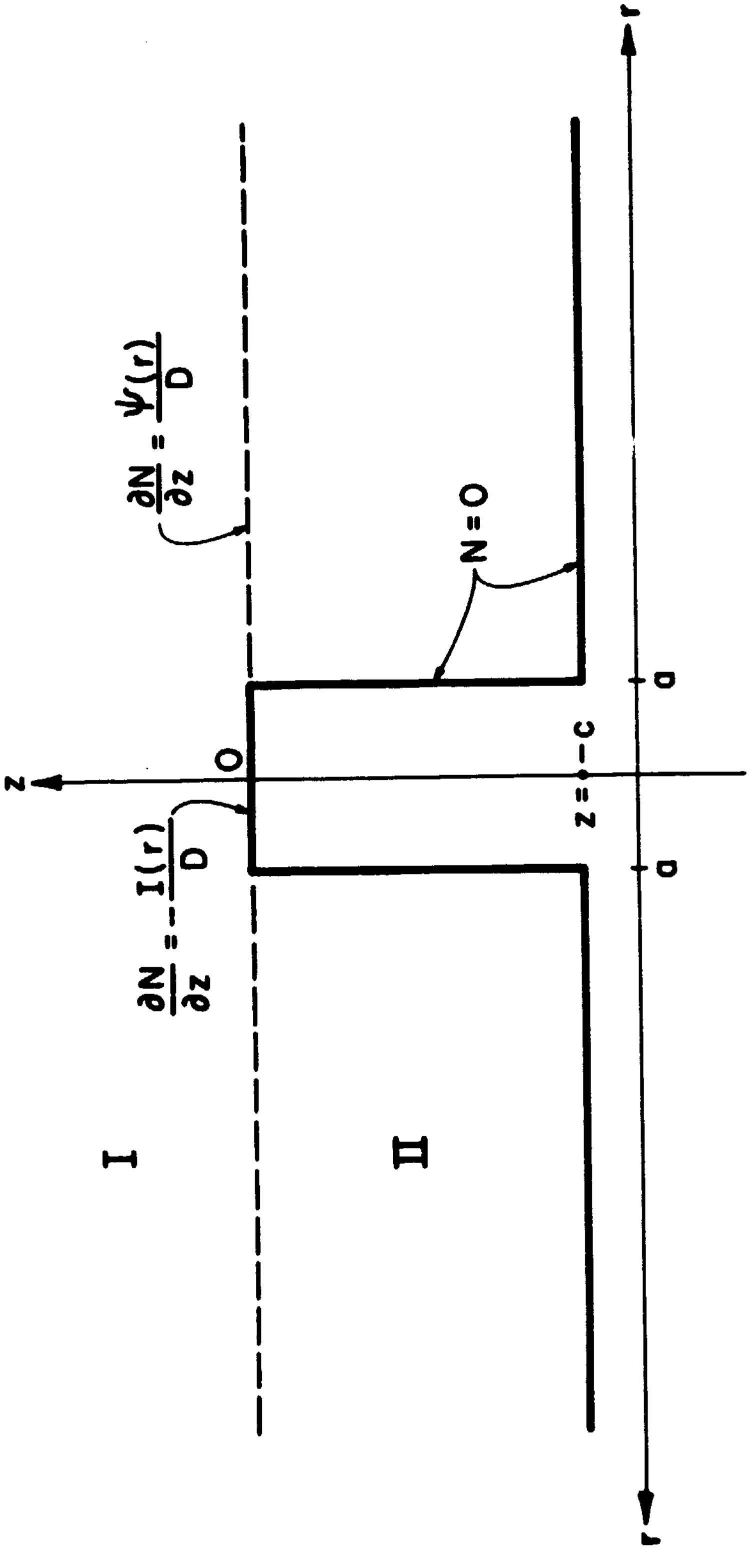
$\frac{\partial N}{\partial z} = \frac{\Psi(r)}{D}$
N = O
$\frac{\partial N}{\partial z} = -\frac{I(r)}{D}$
z
O
z = −c
a
a
r
r
I
II

Figure 2

BOUNDARY-VALUE PROBLEM

In the space $z \geq -c$, let the density of the sputtered atoms be designated by $N(r,z)$ [cm^{-3}] and the flux of emitted atoms at the emitter surface by $I(r)$ [$\mathrm{cm}^{-3} \cdot \mathrm{cm\ sec}^{-1}$]. In steady state, the spatial distribution $N = N(r,z)$ of sputtered atoms is determined by the boundary-value problem for the Laplace diffusion equation (Fig. 2):

$$\frac{\partial^2 N}{\partial r^2} + \frac{1}{r}\frac{\partial N}{\partial r} + \frac{\partial^2 N}{\partial z^2} = 0 \tag{1}$$

where

$$[\partial N(r,z)/\partial z]_{z=0} = -I(r)\overline{D}^{-1}\ H(a-r) \quad , \tag{2}$$

$$N(r,z)_{r=a} = 0 \ , \quad -c \leq z \leq 0 \quad , \tag{3}$$

$$N(r,z)_{z=-c} = 0 \ , \quad a \leq r \leq \infty \quad , \tag{4}$$

and

$$N(r,z) \to 0 \ , \quad (r^2 + z^2) \to \infty \quad , \tag{5}$$

are the proper and improper boundary conditions, respectively. $\overline{D}$ designates the diffusion coefficient of the sputtered atoms in the rarefied plasma which represents a spatial average, $\overline{D} \equiv \langle D(r,z) \rangle$. The Heaviside function is defined as

$$H(a-r) = 1 \ , \quad 0 \leq r < a \quad ,$$

$$= 0 \ , \quad a < r \leq \infty \quad .$$

The boundary conditions (3)-(4) imply that sputtered atoms arriving at the system surfaces are deposited there, i.e., do not return into the diffusion space. This assumption is at least approximately correct for nonheated surfaces as long as the number of atomic layers deposited is not too large. The fluxes $\Phi_i = -D\,\nabla_i N$ of atoms arriving at the system surfaces $r = a$, $-c \leq z \leq 0$ and $z = -c$, $a \leq r \leq \infty$ are given by

$$\Phi_r(r = a,z) = -D\,\partial N(r = a,z)/\partial r\ , \quad -c \leq z \leq 0 \quad , \tag{6}$$

$$\Phi_z(z = -c,r) = -D\,\partial N(z = -c,r)/\partial z, \quad a \leq r \leq \infty \quad . \tag{7}$$

Accordingly,

$$N_{r=a} = -\,2\pi a D \int_{-c}^{0} [\partial N(r = a,z)/\partial r]dz \quad , \tag{8}$$

$$N_{z=-c} = -2\pi D \int_{a}^{\infty} [\partial N(r,z = -c)/\partial z]rdr \quad , \tag{9}$$

are the numbers of sputtered atoms deposited per unit time on the system surfaces $r = a$, $-c \leq z \leq 0$ and $z = -c$, $a \leq r \leq \infty$, respectively. The above boundary-value problem can not be solved directly, i.e., requires a decomposition of the space $z \geq -c$ into appropriate subregions for which the associated boundary-value problems are readily solvable. In this approach the common boundary value at the decomposition plane is determined by an integral equation.

DECOMPOSITION BY ONE INTERFACE

In Fig. 2, the space is decomposed into the regions $I(0 \leq r \leq \infty,\ 0 \leq z \leq \infty)$ and $II(a \leq r \leq \infty,\ -c \leq z \leq 0)$. At the interface, $z = 0$, $a \leq r \leq \infty$, the partial $\partial N(r,z = 0)/\partial z = \psi(r)D^{-1}H(r-a)$ is introduced as the common (unknown) boundary value $\psi(r)$ of the adjacent regions I and II.

Region I. $N_I(r,z)$ is described by Eq. (1), and the boundary conditions (5), and

$$\partial N_I(r,z = 0)/\partial z = -I(r)D^{-1} H(a - r) + \psi(r)D^{-1} H(r - a) \quad . \qquad (10)$$

Accordingly, a solution is sought in form of the Fourier integral $(0 \leq z \leq \infty)$

$$N_I(r,z) = \int_0^\infty A(k)e^{-kz} J_o(kr)dk \quad , \qquad (11)$$

whence

$$- \int_0^\infty k\ A(k)\ J_o(kr)dk = D^{-1} \int_0^\infty J_o(kr)\ k\ dk \int_0^\infty [-I(\alpha)H(a - \alpha)$$

$$+ \psi(\alpha)\ H(\alpha - a)]\ J_o(k\alpha)\alpha d\alpha \qquad (12)$$

by Eq. (10) in accordance with the Hankel transformation. Substitution of the Fourier amplitudes $A(k)$ from Eq. (8) into Eq. (7) gives the solution:

$$N_I(r,z) = D^{-1} \int_0^\infty [I(\alpha)H(a - \alpha) - \psi(\alpha)H(\alpha - a)]\ \alpha d\alpha\ \times$$

$$\int_0^\infty e^{-kz}\ J_o(kr)\ J_o(k\alpha)dk \quad . \qquad (13)$$

$N_I(r,z)$ evidently satisfies Eq. (5) since $J_o(kr) \to 0$ for $r \to \infty$, as well as Eq. (10) since

$$\int_0^\infty J_o(kr)\ J_o(k\alpha)\ dk = \delta(r - \alpha)/\alpha \quad .$$

Region II. $N_{II}(r,z)$ is described by Eqs. (1) and the boundary conditions (3)-(5), and

$$\partial N_{II}(r,z = 0)/\partial z = \psi(r)/D\ ,\ a \le r \le \infty \quad . \tag{14}$$

Accordingly, a solution is sought in form of the Fourier series $(-c \le z \le 0)$:

$$N_{II}(r,z) = \sum_{\nu=1}^{\infty} B_\nu\ J_o(\lambda_\nu r)e^{-\lambda_\nu c}\ [e^{+\lambda_\nu(z+c)} - e^{-\lambda_\nu(z+c)}] \tag{15}$$

where

$$J_o(\lambda_\nu\ a) = 0 \quad . \tag{16}$$

determines the eigenvalues $\nu = 1,2,3,\ldots$ Equations (14)-(15) and the orthogonality relations for $J_o(\lambda_\nu r)$ relate the Fourier coefficients,

$$B_\nu = -\ 2\frac{D^{-1}}{a^2}\frac{\int_a^\infty \psi(r)\ J_o(\lambda_\nu r)r\ dr}{\lambda_\nu(1+e^{-2\lambda_\nu c})J_1^{\ 2}(\lambda_\nu a)} \quad , \tag{17}$$

to $\psi(r)$. Equation (15) evidently satisfies the boundary conditions (3)-(5).

Integral Equation for $\psi(r)$. In the solutions for $N_I(r,z)$ and $N_{II}(r,z)$, the function $\psi(r)$ is still unknown [Eqs. (13) and (15)]. Since the z-derivatives of $N_I(r,z)$ and $N_{II}(r,z)$ have already been matched at the interface, $z = 0$, $a \le r \le \infty$, $\psi(r)$ is determined by the remaining continuity condition,

$$N_I(r,z = 0) = N_{II}(r,z = 0)\ , \quad a \le r \le \infty \quad . \tag{18}$$

Substituion of Eqs.(13) and (15), (17) yields for $\psi(r)$ the integral equation:

$$\int_0^\infty \psi(\alpha)\ H(\alpha - a)\ Q(\alpha,r)\ d\alpha = \sigma(r) \tag{19}$$

where

$$Q(\alpha,r) \equiv \alpha \int_0^\infty J_o(kr)\ J_o(k\alpha)\ dk - 2\frac{\alpha}{a} \sum_{\nu=1}^{\infty} \frac{\mathrm{tgh}\ \lambda_\nu c\ J_o(\lambda_\nu \alpha)}{\lambda_\nu a\ J_1{}^2(\lambda_\nu a)}\ J_o(\lambda_\nu \alpha)\quad , \qquad (20)$$

$$\sigma(r) \equiv \int_0^\infty I(\alpha)\ H(a-\alpha)\alpha d\alpha \int_0^\infty J_o(kr)\ J_o(k\alpha)dk \qquad , \qquad (21)$$

are the kernel and the source of Eq. (19), respectively. Since 2)

$$\int_0^\infty J_o(kr)\ J_o(k\alpha)dk = \frac{2}{\pi}\ [\frac{1}{r}\ K(\frac{\alpha^2}{r^2})\ H(r-\alpha) + \frac{1}{\alpha}\ K(\frac{\alpha^2}{r^2})\ H(\alpha-r)\ , \qquad (22)$$

where $K(m = k^2)$ is the complete elliptic integral of the first kind, $Q(\alpha,r)$ and $\sigma(r)$ become:

$$Q(\alpha,r) = \frac{2}{\pi}\frac{\alpha}{r}\ K(\frac{\alpha^2}{r^2}) - 2\frac{\alpha}{a} \sum_{\nu=1}^{\infty} \frac{\mathrm{tgh}\ \lambda_\nu c}{\lambda_\nu a}\ \frac{J_o(\lambda_\nu a)}{J_1{}^2(\lambda_\nu a)}\ J_o(\lambda_\nu \alpha)\ , \quad r \geq a\ , \qquad (23)$$

$$\sigma(r) = \frac{2}{\pi} \int_0^\infty I(\alpha)\ H(a-\alpha)\ \frac{\alpha}{r}\ K(\frac{\alpha^2}{r^2})d\alpha\ , \quad r \geq a \qquad , \qquad (24)$$

noting that $\alpha \leq a$ and $r \geq a$ along the interface of the regions I and II, and, hence, $r \geq \alpha$ in Eqs. (21)-(22). In case the sputtered atoms are emitted homogeneously, $I(r) = I_o$, Eq. (24) reduces to

$$\sigma(r) = \frac{2}{\pi}\ I_o\ r^{-1}\ [E(\frac{a^2}{r^2}) - (1 - \frac{a^2}{r^2})\ K(\frac{a^2}{r^2})]\ , \quad r \geq a \qquad , \qquad (25)$$

where $E(m = k^2)$ is the complete elliptic integral of the second kind. Note that $\sigma(r = a) = 0$ and $\sigma(r = \infty) = 0$.

From the mathematical point of view, Eqs. (13) and (15, 17), which give the atom density in the space $z \geq -c$, and Eq. (19), which determines the remaining unknown function $\psi(r)$, represent the formal solution of the deposition problem.

FURTHER REMARKS

Attempts at solving the integral equation defined by Eqs. (19) and (23)-(24) in closed form were not successful. Consecutively, the boundary-value function $\psi(z)$ was determined numerically from Eq. (19) by an iteration method. Substitution of a finite number of values $\psi_i = \psi(z_i)$, $0 \leq z_i < \infty$, into Eq. (17) gave (approximate) numerical values for the Fourier expansion coefficients B_ν. The numerical solution $N(r,z)$, obtained by substitution of these B_ν values into the Fourier series in Eq. (15), however, showed insufficient convergence, in particular at the corners of the system (Fig. 2). This difficulty is evidently due to (minor) numerical errors in the computation of B_ν, which are added up in the Fourier series.

In order to find a simpler, analytical solution to the deposition problem, other analytical attempts were made, e.g. by decomposition of the diffusion space into three simple regions through two interfaces (Fig. 3). However, this approach results in an infinite system of algebraic equations and an even more complicated integral equation.

The analysis of the deposition of charged particles, produced by charge-exchange between sputtered atoms and beam ions, leads to a similar outer boundary-value problem for coupled, nonlinear partial differential equations (collision-free electrohydrodynamic equations and Poisson equation). For the latter reason, first the simpler problem of the deposition of neutral atoms by diffusion was treated.

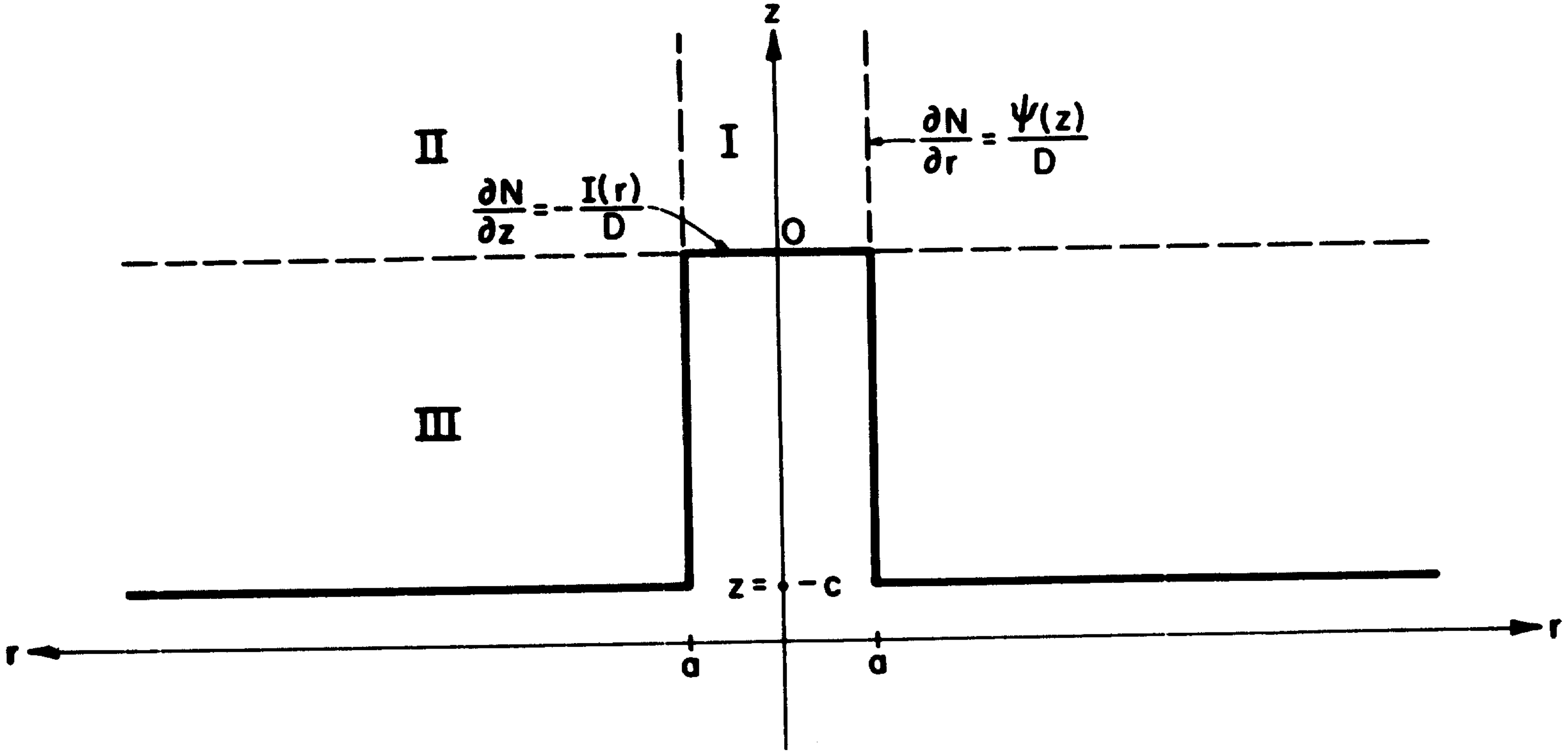
z
II
I
$\frac{\partial N}{\partial r} = \frac{\Psi(z)}{D}$
$\frac{\partial N}{\partial z} = -\frac{I(r)}{D}$
O
III
z = −c
r
r
a
a

Figure 3

Citations

1. A. A. Vlasov, Many-Particle Theory and its Application to Plasma, Gordon & Breach, New York, 1961.
2. M. Abramowitz and I. A. Stegun, Handbook of Mathematical Functions, NBS, Washington, 1966.